NASA CR-179579

Long Term Deposit Formation in Aviation Turbine Fuel at Elevated Temperature

Anthony J. Giovanetti
Eugene J. Szetela

UNITED TECHNOLOGIES RESEARCH CENTER
East Hartford, CT 06108

April 1985

National Aeronautics and Space Administration

Lewis Research Center
Cleveland, Ohio 44135

1. Report No.	2. Government Accession No.	3. Recipient's Catalog No.
NASA CR-179579		

4. Title and Subtitle	5. Report Date
Long Term Deposit Formation in Aviation Turbine Fuel at Elevated Temperature	April 1985
	6. Performing Organization Code

7. Author(s)	8. Performing Organization Report No
Anthony J. Giovanetti Eugene J. Szetela	R85-956648-19
	10. Work Unit No.

9. Performing Organization Name and Address	11. Contract or Grant No.
United Technologies Research Center Silver Lane East Hartford, CT 06108	NAS3-24091

12. Sponsoring Agency Name and Address	13. Type of Report and Period Covered
National Aeronautics and Space Administration Washington, DC 20546	Final Report 11/83 to 3/85
	14. Sponsoring Agency Code

15. Supplementary Notes

NASA-Lewis Research Center, Cleveland, OH 44135
Project Manager, Steve Cohen

16. Abstract

An experimental research program was undertaken to characterize the relationship between deposit mass, operating time, and temperature in coking studies for aviation fuels under conditions simulating those in a modern aircraft turbine fuel system. The rates of carbon deposition in heated stainless steel tubes were determined for Jet A and the alternative fuel Suntech A using a novel steady flow test apparatus which permitted variation and evaluation of the effect on deposit formation of fuel and surface temperature, fuel velocity, and operating time. In addition, the heated-tube data were used to develop a global chemical kinetic model for predicting and correlating deposit formation rates for a range of operating conditions.

Parametric tests to map the thermal stability characteristics of Jet A and Suntech A were conducted at a pressure of 3.4 MPa, fuel velocities of 0.07 and 1.3 m/s, tube wall temperatures in the range of 420 to 750 K, maximum fuel temperatures in the range of 420 to 560 K, and for test durations from 3 to 730 hr. In general, fuel deposit rates were found to be a strong function of wall temperature, and at a common test condition, the rates for Suntech A exceeded those for Jet A by a factor of ten. Unexpectedly, for both fuels, deposit rates increased markedly as test duration increased. A finite-rate chemical reaction model verified the effect of dissolved oxygen in the fuel as a limiting agent for deposit formation, and the importance of the fuel temperature-time history for affecting downstream deposition.

17. Key Words (Suggested by Author(s))	18. Distribution Statement
Aviation fuel, thermal stability, coking, deposit formation, thermal decomposition	Unclassified - Unlimited

19. Security Classif. (of this report)	20. Security Classif. (of this page)	21. No. of Pages	22. Price*
Unclassified	Unclassified		

* For sale by the National Technical Information Service Springfield Virginia 22161

Long Term Deposit Formation in Aviation Turbine Fuel at Elevated Temperature

TABLE OF CONTENTS

FOREWORD

This research was conducted by the United Technologies Research Center, East Hartford, Connecticut under Contract NAS3-24091 from NASA-Lewis Research Center, Cleveland, Ohio. Mr. Steve Cohen was the NASA Project Manager.

The authors acknowledge laboratory technicians Mr. Andrew Robinson and Mr. David Shaw for their assistance in making this program a success. In addition, a special note of appreciation goes to Mr. C. "Buck" Nowack of the Naval Air Propulsion Center, Trenton, New Jersey for his effort in securing the sample of Suntech A used in this research.

Finally, in writing this report, the authors remember our late colleague Dr. Bert Phillips, a former researcher of NASA-Lewis Research Center and participant in this effort, who passed away during this program.

Long Term Deposit Formation in Aviation Turbine Fuel at Elevated Temperature

A. J. Giovanetti
E. J. Szetela

SUMMARY

An experimental research program was undertaken to characterize the relationship between deposit mass, operating time, and temperature in coking studies for aviation fuels under conditions simulating those in a modern aircraft turbine fuel system. The rates of carbon deposition in heated stainless steel tubes were determined for Jet A and the alternative fuel Suntech A using a novel steady flow test apparatus which permitted independent variation and evaluation of the effect on deposit formation of fuel and surface temperature, fuel velocity, and operating time. In addition, the heated-tube data were used to develop a global chemical kinetic model for predicting and correlating deposit formation rates for a range of operating conditions.

Parametric tests to map the thermal stability characteristics of Jet A and Suntech A were conducted at a pressure of 3.4 MPa, fuel velocities of 0.07 and 1.3 m/s, tube wall temperatures in the range of 420 to 750 K, maximum fuel temperatures in the range of 420 to 560 K, and for test durations from 3 to 730 hr. In general, fuel deposit rates were found to be a strong function of tube wall temperature, and at a common test condition, the rates for Suntech A exceeded those for Jet A by a factor of ten. Unexpectedly, for both fuels, deposit rates did not remain constant as a function of test duration. For Jet A, the rates of carbon deposition were proportional to the second power of test duration, i.e., time-average carbon deposition rates were quadrupled as test time was doubled, suggesting that deposit material formed on the tube in the early stages of the test may have provided an active surface which enhanced further fuel deposition. Also, all deposits obtained at the low velocity condition of 0.07 m/s were non-uniform in thickness, cellular in structure, and found to have an average density of 0.08 g/cm^3 based on carbon content. However, at the higher velocity of 1.3 m/s, fuel deposit coverage of the tube was more uniform and a significantly denser deposit having an average density of 0.8 g/cm^3 was observed.

In individual tests where the fuel residence time was sufficiently long at elevated tube temperatures, deposit formation rates reached maximum values at intermediate values of tube temperature and position (e.g., approximately 550 K for a residence time of 5 s and 500 K for 13 s). As fuel residence time

and tube temperature were further increased, deposit formation rates decreased significantly from their maximum values. A possible explanation for this phenomenon was that during the fuel heating process, active oxygenated species (which are precursors to deposit formation) are formed and later depleted as fuel flows through the tube. Based on this hypothesis, a two-step finite-rate chemical reaction model was formulated to simulate the complicated fuel oxidation and deposit formation processes. The results of this model when applied to the heated-tube experiments verified the effect of dissolved oxygen in the fuel as a limiting agent for deposit formation, and the importance of temperature-time history of the fuel for affecting downstream deposition. Further, the model was used to develop a similarity parameter defined as the overall deposition rate constant which in turn was used to correlate in a concise manner the heated-tube deposit data for a range of surface temperatures, fuel residence times, fuel velocities, and test durations. The results of the experimental and modelling efforts provide a basis for the development of a design/application procedure for predicting deposit formation in aircraft fuel systems.

INTRODUCTION

Background

Hydrocarbon gas turbine fuels in contact with heated surfaces form insoluble, carbonaceous deposits which often plug fuel passages in heat exchangers, fuel manifolds, and injectors. The chemical changes resulting in deposit formation are not understood, but it is believed that oxidation processes leading to the formation of free-radical species are involved (Ref. 1). The deposit process is slow yet observable at temperatures in the range 450 to 500 K. Above 600 K, the process becomes substantially more rapid (Ref. 2).

A reliable correlation of the growth of deposits with operating conditions including temperature, run time, and velocity is required by fuel system designers to prevent deposit build-up in fuel system components. Such a correlation has not been available although a number of investigators have studied deposit formation in previous programs. One of the techniques used to qualify the extent of carbon deposition was to measure the rise in surface temperature with time and deduce the thermal resistance (Refs. 3 and 4); however, deposit mass cannot be directly obtained from the data. Deposit mass has been characterized by oxidizing the deposit and measuring CO and CO_2 concentrations in a number of investigations which involved tests of 10 min to 100 hr duration (Ref. 5-10). It was found that deposit formation rate is strongly dependent on temperature, but the effect of run time could not be discerned. Another technique was to measure deposit thickness directly by a micrometer method, and thicknesses up to 0.02 mm were reported after cyclic tests in a fuel system simulator which was operated for 250 hr (Ref. 11). A beta-ray technique was used to analyze heated tube specimens run at temperatures between 900 and 1000 K for periods up to 100 hr (Ref. 12), but these data are not directly applicable to gas turbine fuel systems.

Program Description

The purpose of the present program was to determine the relationship between run time and temperature on the deposit buildup resulting from the flowing of Jet A fuel in a heated tube. Also, the alternative lower quality fuel Suntech A was tested. The program included the design, fabrication, and operation of a novel thermal stability test apparatus, the determination of deposition rates over a range of temperatures and test durations, and the development of correlations relating short duration, high-temperature results to data obtained at lower temperatures over long durations. The method of approach to accomplish these tasks consisted of (1) characterizing each test fuel with respect to its chemical composition, physical properties, and thermal stability as determined from the ASTM Jet Fuel Thermal Oxidation

Tester (JFTOT), (2) designing and fabricating a heated-tube test apparatus for determining the thermal stability of the fuels from 350 to 560 K bulk fuel temperature, (3) thermally stressing each test fuel in accordance with a prescribed matrix of operating conditions, including tests to establish adequate precision of the apparatus, (4) characterizing the levels of carbon deposition observed in the experiments, and (5) correlating the deposit formation data in a format which includes the effects of surface temperature, operating time, and fuel velocity (residence time).

The organization of this report is as follows: First, a section is presented which describes the experimental approach including the fuels characterization analysis, test apparatus and test procedures, and test matrix. Next, the measured carbon deposition rate data is presented, and the important trends are identified and correlated with the experimental conditions. In addition, a chemical kinetic reaction model is developed and applied to the tube-generated deposition data. In conjunction with the model, a correlation is developed which predicts carbon deposition rates for a range of test conditions and includes the effects of surface temperature, fuel temperature-time history, and fuel velocity. Finally, the last section of this report summarizes the important conclusions of the program.

EXPERIMENTAL APPROACH

Experiments were conducted in heated tubes to evaluate the rates of carbon deposition for Jet A and Suntech A in tests up to several hundred hours duration and under flow and temperature conditions simulating the fuel system of a modern aircraft gas turbine engine. The fuel characteristics, test facility, and data analysis procedures are discussed in the following sections.

Fuels Characterizations

Each fuel used in the program was withdrawn as a single batch from a large supply and stored in unused steel drums under an unheated outdoor protective enclosure. The Jet A (Aviation Turbine Fuel Specification ASTM D 1655) was acquired from a local gas turbine development testing facility, and the alternative fuel, Suntech A, (designated by the Government as NAPC-19) was supplied by the Naval Air Propulsion Center. The chemical and physical properties and thermal stabilities of each fuel were obtained by providing samples to independent analytical laboratory facilities, i.e., chemical composition and physical properties analyses were performed by Southern Petroleum Laboratories, Inc., and fuel thermal stability testing for breakpoint temperature determination using the ASTM Jet Fuel Thermal Oxidation Tester (JFTOT) were done at Southwest Research Institute. Table I summarizes the results of the fuels characterization analyses, including the particular ASTM test method used for each determination. Also, for both fuels, Table II provides as a function of temperature the approximate values for density, specific heat, thermal conductivity, and absolute viscosity used to compute the flow parameters for each test (e.g., Reynolds number, local velocity, and heat flux).

As shown in Table I, there is an anomaly in the thermal stability between Jet A and Suntech A with respect to the differences in their chemical compositions, i.e., aromatics from 21 to 40 percent, sulfur from 0.05 to 0.24 percent, and nitrogen from 12 to 250 ppm for Jet A and Suntech A, respectively. Because the latter species are generally regarded as detrimental to fuel thermal stability, Suntech A would have been expected to exhibit a lower breakpoint temperature (actual value = 538 K). Also, it is worth noting that the Jet A fuel sample had a total aromatic content in excess of 20 percent by volume and had a relatively low thermal stability breakpoint temperature, both of which classify the fuel as marginal in passing the Jet A fuel specification.

Test Apparatus and Test Procedures

Apparatus

A novel fuel thermal stability test apparatus, shown schematically in Fig. 1 and photographically in Fig. 2, was developed to provide fundamental information on fuel deposition rates over a wide range of temperatures, test durations, and flow rates. The apparatus consists of multiple resistance-heated, stainless steel tubes which are connected in series with unheated constant temperature (isothermal) tubes. Because of the planned long duration tests and the considerable effort required to run them, multiple tubes were chosen to permit tests of different durations to be run concurrently, thereby maximizing data output. In addition, the apparatus features metal wafer specimens and water-cooled deposit collection filters immersed in the fuel stream downstream of each tube section. The heated-tube sections provide information on the deposit formation that occurs when the temperature differential between the surface and fuel is large (approximately 100 K), whereas the isothermal tubes and metal wafer specimens yield data for the condition when the surface and fuel temperatures are equal. The water-cooled deposit collection filters enable determination of the combined masses of residual deposit which forms and remains in the bulk flow and the deposit which breaks away from upstream tube sections.

The experimental apparatus was designed so that all components directly in contact with the fuel were constructed from either stainless steel, steel, plastic, or aluminum, and as shown in Fig. 1 consists of: (1) a fuel supply tank and sparging element to saturate the fuel with air prior to test; (2) a zeolite-type molecular sieve used to remove water and gum deposits from the fuel; (3) a fuel delivery system comprising four piston-type accumulators which are used to drive fuel through the test section; (4) a calibrated flow metering orifice at the inlet of each heated tube to maintain identical flow rates in each tube; (5) a test section comprising three resistance-heated tubes connected in parallel to an a-c power supply, followed by three isothermal tubes; (6) stainless steel wafer specimens immersed in the fuel stream at locations immediately upstream and downstream of each isothermal tube; (7) a water-cooled, nominal 15 μm sintered, stainless steel deposit collection filter at the outlet of each isothermal tube for use in selected tests; (8) a fuel cooler; (9) an electrically-driven metering valve and turbine flow meter to control and monitor the total fuel flow rate through the test section; and (10) a fuel collection tank. The apparatus is located in a concrete test cell, and the associated control and data acquisition systems are remotely located in a separate control room. It is capable of continuous operation at maximum fuel temperatures and pressures up to 500 K and 3.4 MPa for fuel flow rates up to 14 kg/hr per tube.

Each of the three test tube assemblies shown in Fig. 1 is fabricated from 0.22-cm ID x 0.32-cm OD, 316 stainless steel tubing. The 0.91-m-long resistance-heated tube subassembly is brazed to copper electrodes which attach to the 8 kVA a-c power supply, and the connecting 0.30-m-long isothermal tube subassembly is enclosed in a concentric, cylindrical ceramic oven to compensate for heat losses to the environment. Outer tube wall temperatures are measured using eleven chromel-alumel thermocouples which are spot welded to the outer wall of the heated tube at equal spacings of 7.6 cm. The thermocouple junctions are coated with Sauereisen cement to insure good thermal contact and to minimize heat conduction losses. In the same manner, five thermocouples, spaced at 5.1-cm intervals, are attached to each isothermal tube. The use of an a-c power supply to heat the tubes assures that temperature measurement errors resulting from a voltage drop across the thermocouple bead are minimized. Because radial temperature gradients are usually negligible across the tube wall (i.e., at low heat flux), to a first approximation the outer wall temperature equals the inner wall temperature. The inlet and outlet fuel bulk temperatures from the heated and isothermal tubes are measured using duplicate small diameter (0.051 cm) thermocouples inserted into special instrumentation plenums which also contain the 0.64-cm-long x 0.32-cm-wide x 0.005-cm-thick 316 stainless steel wafer specimens. Since piercing the tubes for insertion of thermocouples at intermediate stations is not considered to be good practice (because of possible fuel leakage, insertion of preferential sites for deposition, and electrical discontinuities) fuel temperatures at intermediate stations are calculated, assuming the fuel enthalpy increases linearly with tube position for uniform heat flux distribution and using the fuel enthalpy vs. temperature data of Table II.

The test tube assemblies are electrically isolated, mounted vertically, and wrapped in blankets of Fiberfrax insulation to reduce heat losses. The vertical orientation causes the buoyancy forces acting on the fuel (due to the induced axial temperature gradient) to be in the same direction as the flow, thereby suppressing any secondary flow motion that would occur at a very low Reynolds number (e.g., inlet Re = 70 at 0.07 m/s velocity).

The fuel inlet pressure, the pressure loss across each heated tube, and the pressure loss across each isothermal tube and deposit collection filter subassembly are monitored continuously using strain-gauge-type pressure transducers and multiple port pressure tap selector valves. Individual tube flow rates are determined from the measured pressure drops across the calibrated metering orifices, and the downstream turbine meter provides the total flow rate and a consistency check of the value obtained by summing the individual orifice flow rates (usually within 5 percent). Total electrical power to the heated tubes is monitored using an inductive current pickup and voltage transducer. However, because of unavoidable heat losses from the tubes to the environment, the actual heat flux applied to each tube is determined from the rise in fuel temperature (i.e., sensible enthalpy) across each heated-tube section.

All test data are recorded using a calculating data-logger microprocessor. The data system converts the output signals from thermocouples pressure transducers, current transducers, voltage transducers, and flow meters to precisely scaled d-c voltages for measurement, but displays the data in engineering units through built-in linear scaling functions. A built-in cathode ray tube provides a continuous display of selected operating variables. The data are recorded automatically at preprogrammed intervals on paper, and if desired, magnetic tape and are subsequently reduced on a high-speed digital computer.

Test Procedures

A standard procedure is used for tube fabrication and installation. Prior to installation, the inside of each tube subassembly is rinsed with acetone and air dried. In addition, the stainless steel wafer specimens are cut to size from sheet material, degreased by soaking in acetone, rinsed with distilled water, and placed into labelled glass vials for cataloging. The wafer specimens are dried by placing the glass vials in a vacuum furnace maintained at 370 K. After weighing each clean wafer specimen on an analytical balance to the nearest 10 μg, it is crimped in place in a special holder which in turn is installed inside its respective thermocouple instrumentation plenum. During the cleaning, weighing, and installation operations, care is taken to handle the wafer specimens using only degreased tweezers to avoid contamination prior to test.

Routine pretest facility preparation consisted of installing clean test tubes, wafer specimens, deposit collection filters, cleaning the upstream fuel filters with a solvent, and verifying proper operation of the control and data acquisition systems. Prior to refueling the piston accumulators, the fuel in the supply tank is aerated by forced circulation through an inline, sintered stainless steel sparging element connected to a filtered air supply. The level of dissolved air in the fuel is known to affect the deposit forming potential of the fuel, and the air sparging operation assures that all the fuel used in the experiments has the same level of dissolved air, i.e., as close to the saturation value as possible. The sparging element is an effective device for air saturating the fuel because it provides a high surface area to volume ratio which promotes intimate contact between the fuel and air. Typically, the sparging process is continued until the volume of fuel to be loaded into the accumulators passes through the element seven times.

After pressurizing the accumulators with the nitrogen driver gas, the test pressure and flow rate are established in the tubes and the entire system is inspected for fuel leaks. Provided there are no leaks, the test is initiated by applying power to preheat the isothermal tube oven heaters. After about 20 min, the primary electric power supply used to heat tubes is activated, and slowly increased to heat the flowing fuel to the desired

temperature. Total transient time from test initiation to the temperature setpoint is typically 30 to 45 min.

During most of the tests, the fuel flow rate and inlet and outlet fuel temperatures (hence, input electrical power) are identical and maintained constant for the three tubes. A proportional fuel temperature controller and silicon crystal rectifier maintain constant the a-c electrical power to the tubes, and the electrically-driven fuel metering valve coupled to a meter relay responds to the output of the turbine flow meter to hold the total flow rate constant (the metering orifices assure identical flow rates between tubes). In some runs, a ballast resistor connected in series to one of the tubes is used to reduce its heat flux by 15 percent with respect to either of the other two tubes. Therefore, the apparatus permits data to be obtained simultaneously for three tubes at identical flow rates and two heat fluxes. In addition, all control systems are coupled to an interlock system, and if any critical operating parameter (i.e., fuel pressure or tube temperature) should vary outside of a specified range, automatic shutdown would be initiated, thereby providing for safe, unattended operation during extended duration runs.

In order to run several test durations at a prescribed flow and temperature condition, tests are usually run using a set of five tubes; three of which are installed in the multiple-tube apparatus initially. The apparatus is operated continuously until enough time has elapsed for one of the tubes to attain its targeted duration, or until a portion of it completely fouls with deposit. At this point, the apparatus is shut down, and the tube and its wafer specimens are removed and replaced with one of the clean assemblies. The apparatus is restarted and the test continues until a second shutdown, at which a second tube is removed and replaced with the remaining clean assembly. The apparatus is then run until final shutdown. Test shutdown is initiated by turning off electrical power to the tubes and maintaining fuel flow for 45 min to permit sufficient time for the high heat capacitance ceramic ovens to cool to ambient temperature, assuring that when fuel flow is terminated, no additional coking occurs in the fuel trapped in the isothermal tubes. After final shutdown, all tubes and related specimens are removed, cataloged, and stored for post test analysis. Deposit wafer specimens are returned to their respective storage vial and maintained under a blanket of low-pressure nitrogen, and tubes are cut from the apparatus and stored in plastic bags at room temperature.

Because of their relatively low surface area which resulted in a short fouling time, deposit collection filters were installed during the initial portions of only a few selected tests to document the amount of deposit material carried in the fuel stream relative to the amount formed on the upstream tube sections. At any condition run in this program, significant deposit (i.e., enough to cause excessive pressure losses and prevent further operation of the apparatus) was trapped on each deposit collection filter in about 6 hr after test startup. Once the filters were removed, the test was continued without installing replacements.

Deposit Characterization and Data Reduction

The quantity of carbon deposited in each tube and on each deposit collection filter is measured by oxidizing the deposit in oxygen with analysis of the evolved CO_2. The amounts of total deposit (carbon and other constituents) formed on the stainless steel wafer specimens are determined by weighing them prior and subsequent to test. Prior to analysis, all tube, filter, and wafer specimens are vacuum dried at 370 K for about twelve hours to remove any residual liquid fuel.

As shown in Fig. 3, equally-spaced sections (each approximately 6.4 cm long) are cut from the heated and isothermal tubes and used in the deposit oxidation analysis; other sections of the tubes are sliced into longitudinal sections which are mounted, polished, and examined microscopically. A special tube holding fixture and jewelers saw are used to section the tubes. The numbers indicated on the individual tube sections of Fig. 3 identify the positions of the sections as measured in inches from the inlet of the heated tube.

The deposit oxidation apparatus, shown schematically in Fig. 4, is designed to permit the simultaneous analysis of several deposit specimens through the use of individual sampling lines arranged in parallel and placed within a common furnace. After the tube or filter sections are installed in the high-temperature (approximately 870 K) laboratory furnace, each deposit is reacted with a separately metered flow of oxygen directed through the inside of the tube. The effluent gas stream from each individual tube specimen passes through a platinum/palladium catalytic converter to ensure complete oxidation of all carbonaceous species to CO_2, and collects in a previously evacuated glass flask for subsequent analysis. The concentration of CO_2 in the product gases is continuously monitored using an online, nondispersive infrared analyzer, and the burnoff process continues until there is no evidence of further evolution of CO_2. At the conclusion of the burnoff, the total mass and average composition of the product gases collected from individual tube specimens is determined, and the mass of carbon in each deposit specimen is calculated from a mass balance.

The minimum carbon mass that could be accurately measured on a standard tube section using the deposit oxidation apparatus was determined to be 200 μg, and the weighing procedure used for the wafer specimens was accurate to the nearest 10 μg. Also, the accuracy of the deposit oxidation apparatus was validated by performing several calibration runs during the program in which preweighed samples of spectrographic-grade carbon (ranging from 4 to 12 mg) were oxidized. Agreement between the amount of carbon input and the amount calibrated in the exhaust products was ± 5 percent for 75 percent of the calibration samples tested.

The carbon mass as determined from the deposit oxidation analysis is used to compute the normalized rate of carbon deposition defined as the mass of carbon divided by the inside lateral surface area of the tube section and the total test time; and it is expressed in units of $\mu g/cm^2$-hr. Since the accumulation of deposit on the tube wall reduces the inside lateral surface area, an average of the clean tube area and final deposit area was used in calculating the rate of carbon deposition parameter. This was accomplished by examining microscopically at low power (32 X) several longitudinal tube sections (Fig. 3) from selected tests, measuring the average deposit thicknesses, and using the tube deposit mass determinations to compute a deposit density. Because the deposit density was found to be invariant for tests run at the same fuel velocity, effective deposit thicknesses and average surface areas were in turn calculated for all specimens processed through the deposit oxidation technique.

Due to the large number of specimens generated in the program, the deposit rate and effective thickness calculations were automated using a computer program. In addition, the computer program collated in concise summary tables the online temperature and flow data time-histories from the tube tests with the deposit mass determinations.

Test Matrix

The test matrix, shown in Tables III-A and III-B, comprised twenty-nine tests for Jet A and Suntech A. A test code identifies each separate run and provides an implicit summary of the experimental conditions for that run (see footnotes at the bottom of Tables III-A and III-B). The test conditions were chosen to provide a data base for fuel deposition in internal flow passages under forced-convective conditions simulating the environment of a modern aviation gas turbine fuel system. The objective was to develop a correlation relating accelerated testing deposit formation data at high temperature to long term coking (hundreds of hours) at more moderate temperatures. Ultimately, this information could be incorporated into a design algorithm for use in predicting coking rates in fuel system components under service conditions. Individual tests were designed to elucidate the effects of (1) wall temperature, (2) wall-to-bulk fuel temperature difference, (3) fuel velocity, (4) fuel residence time during heating, and (5) total test (operating) time.

All tests were conducted at the nominal inlet conditions to the heated tube consisting of a pressure of 3.4 MPa and a fuel temperature of 290 K for heat fluxes between 0.9 and 30 W/cm^2. Long-term tests with durations ranging from 50 to 730 hr were run at a fuel inlet velocity of 0.07 m/s (flow rate = 0.73 kg/hr at Re = 70) and maximum fuel temperatures at the heated tube outlet

of 420 and 450 K. Short term tests lasting under 50 hr in duration were run at fuel inlet velocities of 0.07 m/s and 1.3 m/s (flow rate = 13.2 kg/hr at Re = 920) and maximum fuel outlet temperatures of 420, 490, 505, and 560 K. Because the fuel pressure throughout the tube was maintained above the critical pressure (2.2 MPa) and the maximum tube temperature usually did not exceed the critical temperature (670 K), the fuel was in a compressed liquid state.

The program began by conducting a series of short-duration tests (not shown) using Jet A to establish the operating characteristics of the multiple tube experimental apparatus, including the degree to which conditions in individual tubes could be maintained identical, and to verify proper operation of the associated data acquisition and automatic control systems. As a result, flow (velocity) and temperature conditions between tubes were found to be identical to within 5 percent. Subsequent to these evaluations, a series of precision tests using three tubes (see Runs 5 to 7, Table III-A) were conducted at a condition where the fuel outlet temperature was held at 560 K for 20 hr. At the end of these tests, sections from three selected tube positions (-18, -21, -24 stations in Fig. 3) were cut from each tube, and the deposit formation rates for each of these sections were characterized using the deposit oxidation procedure. At each of the three tube positions, the variation in the carbon deposition rates between tubes did not exceed 22 percent, with 75 percent of the specimens analyzed falling within a bandwidth of 10 percent.

EXPERIMENTAL RESULTS AND DISCUSSION

In this section, the data for the heated-tube tests and the deposit mass loading characterizations conducted for Jet A and Suntech A are presented. Based on the trends common to all the experimental data, a two-step chemical reaction is formulated and applied to a well-stirred reactor model of the tube experiment to predict fuel oxidation and deposit formation as a function of temperature and residence time. In turn, the reaction model provides a similarity parameter ressembling an overall deposition rate constant which is used to correlate the data in a form accounting for the combined effects of fuel temperature-time history (residence time), test duration, and local surface temperature.

Deposit Formation Data

Tube Wall Temperature and Fuel Velocity Distributions

Figures 5 through 7 summarize the wall and computed fuel temperature distributions as a function of time along the heated and isothermal tubes for selected tests showing the full range of conditions run for Jet A and Suntech A; i.e., low velocity (0.07 m/s) and high velocity (1.3 m/s) data for Jet A in Figs. 5 and 6, respectively and low velocity data for Suntech A in Fig. 7. Also, Fig. 8 shows the fuel axial velocity distributions for the heated and isothermal tubes which were calculated using the fuel temperature profiles in Figs. 5 through 7 and the fuel density information given in Table II. Figures 5 and 7 are for the condition where the flow remains laminar ($Re < 2000$) along the entire length of tube, and Fig. 6 denotes a condition where the flow transitions from laminar to turbulent at about 20 cm from the inlet. The laminar flow data of Figs. 5 and 7 are characterized by tube wall temperatures that increase monotonically and almost linearly with axial position, whereas the data of Fig. 6 exhibit a sharp peak in wall temperature in the inlet region and has been observed elsewhere (Ref. 9).

Because the applied heat flux and fuel flow rate to the tube remain constant over time, the rise in initial wall temperature shown in Figs. 5 through 7 is a result of an increase in effective thermal resistance owing to the extent of the growth of deposit on the inside tube surface, i.e., the greatest relative wall temperature increase corresponds to the thickest deposit. Also, because of the relatively low heat fluxes tested in this program, the radial temperature gradients across the tube wall are negligible. Therefore, to a first approximation, the outer wall temperature equals the inner wall temperature, and the temperature at the interface between the fuel and the deposit layer which forms equals the initial inner wall temperature.

Although deposit formation is known to be an increasing function of temperature, Figs. 5 through 7 indicate that the greatest rise in wall temperature (hence, the thickest deposit formed) does not always occur on the section of tube operating at the highest wall temperature. In fact, as seen for the high temperature, low velocity cases (Figs. 5 and 7), maximum increases in wall temperature are observed at an intermediate wall temperature which occurs at a position about 55 cm from the inlet. Downstream of this location, wall temperatures remains nearly constant over time and suggests no deposit forms. As will be discussed later, the rates of carbon deposition for these runs reach a maximum at this tube position, and it is believed that this phenomenon is related to the degree of oxidation the fuel has undergone in upstream sections of the heated tube. Also, for the high velocity run shown in Fig. 6, the accumulation of deposit in the inlet section of the tube moves the sharp peak in the initial wall temperature profile to an upstream position. This may be attributed to the increase in surface roughness from deposit growth and its effect on the energy transport occurring in the viscous sublayer of the turbulent velocity profile. The effect of surface roughness is more apparent in turbulent flow because the viscous sublayer of the turbulent velocity profile is many times thinner than that in the laminar case (a factor of fifteen at Re = 2000).

Effect of Fuel Velocity on Deposit Density

The distinct characters of the Jet A and Suntech A fuel deposits obtained on the tubes as a function of fuel inlet velocity are shown photographically in Figs. 9 (longitudinal sections) and 10 (transverse sections) at a common test condition consisting of an initial tube temperature of about 580 K. A section of clean tube is also shown for comparison in Fig. 9. As shown in the figures for the low velocity condition (0.07 m/s), the deposit appears cellular with a structure that could be described as filamentous. The carbonaceous mass is irregular and often appears as lumps. However, for Jet A at high velocity (1.3 m/s), coverage of tube surface by deposit is more uniform, and the deposit appears amorphous. The higher wall shear associated with this condition probably suppresses growth of the cellular deposit characteristic of the low velocity. Using the deposit thicknesses as measured from the photographs in Figs. 9 and 10 and the deposit mass loading information from the oxidation analyses, the average deposit densities are 0.08 g/cc and 0.8 g/cc based on carbon content for the low and high velocity conditions, respectively. Consequently, even though the deposit mass loading per unit area is nearly the same on each of the tube sections shown in Fig. 10, the apparent deposit thickness is significantly greater for the low velocity specimen because of the lower deposit density.

Rates of Carbon Deposition for Jet A at Low Velocity

Using the deposit oxidation analysis procedure described earlier, the rates of carbon deposition were evaluated for a large number of 6.35-cm-long tube sections for the runs shown previously in the comprehensive test matrix

(see Tables III-A and III-B). The time-average rates of carbon deposition for Jet A at low velocity (0.07 m/s) and for long duration (test duration > 50 hr) are plotted as a function of initial wall temperature in Fig. 11. Only data from the heated tube portion of the experiment is shown; the isothermal tube data will be discussed later. The selection of the initial wall temperature as the correlating parameter assumes that (1) the deposition reaction occurs at the interface between the fuel and deposit layer which forms inside the tube, (2) the initial clean tube wall temperature equals the temperature at the interface between the fuel and the deposit layer because the heat flux and flowrate applied to the tube are constant with time, and (3) the measured outer wall temperature is approximately equal to the inner wall temperature because of the negligible thermal resistance of the tube wall. Because wall temperature is proportional to the distance from the heated-tube inlet (see Fig. 5), Fig. 11 can be thought of as a plot of deposit rates vs. axial position along the tube.

At a given test duration, Fig. 11 shows a trend of monotonically increasing rates of carbon deposition to a peak value with increasing tube wall temperature (position) in the range of 425 K to 500 K, and at temperatures above 500 K, deposit rates decrease slightly from their peak values. As can be determined from Fig. 8, the residence time of the fuel in the tube prior to this peak is about 13 s, and this trend has been observed previously in experiments with heated tubes (Ref. 9). The reasons for the shape of the curve have not been established with certainty, but it is believed that as the fuel is heated, active oxygenated species such as hydroperoxides (which are precursors to deposit formation) are formed and depleted along the tube, and provided the dissolved oxygen concentration in the fuel, the tube wall temperature, and fuel residence time during heating are sufficiently high, a maximum will occur in the deposit rate vs. temperature relationship.

The deposit produced in the tests plotted in Fig. 11 were similar in appearance to those shown for the low velocity condition for Jet A in Figs. 9 and 10. Deposit thicknesses in excess of 0.05 cm (one-quarter of the tube inside diameter) were common over a significant portion of the tube for test durations greater than 100 hr. In fact, plugging of the tubes (which forced test termination) occurred at the outlet of the heated tubes for the 157, 640, and 730 hr tests. Also, a good example of the repeatability of the data is shown by examining the close correspondence between the deposit rates for the 640 and 730 hr tests and the data points for the 157 hr test where in the latter the results from two tests are shown (Runs 11 and 12, Table III-A).

The effect of test duration on deposit rates is also evident in Fig. 11 which shows an apparent increase in the rates of carbon deposition for a fixed value of wall temperature as test duration increases, i.e., the total deposit produced does not scale linearly with test duration. This effect is shown more clearly in Fig. 12, where the deposit mass loading (mass of deposit per unit surface area) data used to construct Fig. 11 have been integrated to

produce a plot of cumulative deposit as a function of position along the tube, i.e., initial wall temperature. Where necessary, the data of Fig. 11 have been extrapolated to encompass portions of the heated tube not analyzed for deposit mass to produce the continuous curves shown in Fig. 12. As is evident from Fig. 12 at a fixed value of wall temperature, deposit formation accelerates at a nonlinear rate with respect to test duration, and as will be shown later, the total deposit produced scales with approximately the third power of time. Also, it is interesting to note in Fig. 12 that although the 640-hr and 157-hr test tubes are operated at slightly different wall temperatures, the total deposit to produce plugging in each is the same.

Similarly, the rates of carbon deposition (Fig. 13a) and cumulative carbon deposit (Fig. 13b) are plotted as a function of initial tube wall temperature for Jet A at low velocity and short duration (4 to 20 hr). Contrary to the longer duration test data of Fig. 12, which were conducted at a lower range of wall temperature, Fig. 13 indicates that for tests lasting between 4 and 20 hr and for wall temperatures in the range of 500 and 625 K, the rates of carbon deposition do not increase with time; therefore, the total carbon deposited in the tube is proportional to test time. Also, the maximum deposit thicknesses observed for the tests shown in Fig. 13 did not exceed 0.05 cm. Because the structure of the deposit produced at low fuel velocity is cellular having a significant internal surface area, previously formed deposit on a section of tube could become active and serve to enhance further deposition. This enhancement effect would be expected to be greatest for the longer duration tests where thick deposits exist for a significant portion of the total test duration. Also, the presence of a defined maximum at about 550 K in the deposit rate vs. temperature curve of Fig. 13a occurs at the point where the fuel residence time is about 5 s and is more apparent than in Fig. 11. Based on the previous discussion regarding the formation and depletion of active oxygenated species along the tube, it is expected that this maximum would be more pronounced at higher wall temperatures.

Note that the data shown for the 20-hr condition in Fig. 13a comprise three separate runs (Runs 5 through 7, Table III-A) and indicate the relatively good precision for most of this experiment. However, the deposit rate data for wall temperatures below 490 K are scattered because the masses of deposit produced on these tube sections approach the minimum value for which the deposit oxidation procedure yields accurate results.

Effect of Test Duration on Deposit Formation

In order to more fully investigate the effect of test duration on deposit formation rate, a composite plot of the smoothed long and short duration data for Jet A at low velocity is shown in Fig. 14. Where the data are nonmonotonic, only the region where deposit rate increases with temperature are

shown. These data (Fig. 14) can be considered to have a more general application than the data in regions where deposit rate decreases with temperature such as in Fig. 13. The later data are too closely related to residence time of the fuel in the tube to be of general value.

It can be seen in Fig. 14 that run time has a significant effect on deposit rate, and this effect is explored further by crossplotting the data in Fig. 14, transforming the deposit rate to a deposit mass loading, and replotting this parameter against run time in Fig. 15. The average slope of the lines in Fig. 15 at constant wall temperature is three, i.e., deposit mass increases with the third power of time. As presented earlier, one possible explanation for this nonlinear behavior is that the surfaces produced by the deposit may become active and result in a rapid increase in deposited mass. A similar set of lines produced by plotting deposit thickness against run time, assuming constant specific gravity of 0.08, is shown in Fig. 16. It can be seen that deposit thickness reached values in excess of 0.1 cm which resulted in plugging of the tube.

A question arises as to whether the apparent nonlinear relationship between deposit formation and test time presented in Fig. 15 is affected by the manner in which the data are plotted. Earlier, it was postulated that the tube initial wall temperature is the appropriate correlating parameter for the deposition data because when the heat flux and flow rate applied to the tube are held constant, the temperature of the interface between the fuel and the deposit which forms is always equal to the initial clean tube wall temperature. This contention is only valid for formation of nonporous, thin, uniform thickness deposits where all additional deposit forms on the exposed surface. However, it would not hold for thick, highly cellular deposits (such as those observed in these experiments) having significant internal temperature gradients. Because the inside temperature of the surface of the deposit adjacent to the tube wall is rising with time (due to the increase in thermal resistance from the accumulation of deposit), the additional deposit which forms in the stagnant fuel trapped in the void volumes of a porous deposit may be produced at an effective temperature which is significantly greater than the initial wall value (as much as 70 K in Fig. 5). In order to explore the magnitude of this effect and its influence on the conclusions, selected deposit rate data from Fig. 11 are smoothed and replotted in Fig. 17 as a function of both final wall temperature and initial wall temperature. Correlating deposit rates with the final wall temperature (that temperature measured at the completion of the test), simulates in an extreme way the effect of rising wall temperature on deposit formation. As seen in Fig. 17 for the correlation with respect to the final wall temperature, the deposit formation rates are shifted so that the apparent trend of increasing rates at a fixed wall temperature for increasing test durations is not as significant as for the correlation with initial wall temperature. Although the plot is inconclusive, it suggests the importance of data interpretation with respect

to the experimental conditions. Also, as will be presented next, the deposit rate data for the isothermal tube specimens, where wall temperature rather than heat flux was maintained constant with time, did not exhibit an apparent dependency on test time.

Deposit Formation on the Isothermal Tube, Filter, and Wafer Specimens

For the several selected tests in which deposit filters were installed, the carbon mass trapped in the filters amounted to no more than 10 percent of the combined mass found on the upstream tube surfaces; suggesting that for the conditions tested in this program, little residual deposit remains in the bulk flow or breaks away from the tube surface. Also, as presented earlier, the 316 stainless steel wafer specimens installed in the fuel stream at the inlet and outlet of each isothermal tube assembly were used to determine the total mass of deposit (carbon plus other constituents) which forms on a hot metal surface. This information was compared to the carbon deposition data from adjacent sections of isothermal tube (which were operated at comparable temperatures) in order to quantify the mass fraction of carbon present in the deposit. Based on this comparison which was done for a range of temperature, the mean mass fraction of carbon in the deposit was estimated to be no more than 65 percent. Finally, because of the complicating effects of suspected active species depletion and its effects on downstream deposition for many of the tests, it was difficult to use the isothermal tube data to assess the effect of fuel temperature on deposit formation. However, in tests which did not show an effect of depletion of species in the heated tube, deposit rates were the same at any wall temperature common to both the heated and isothermal tubes despite significant differences in their respective local fuel temperatures (see Figs. 5 and 6). This observation suggests that wall temperature is the more significant correlating parameter, but any conclusion discounting the effect of fuel temperature on deposit formation is unwarranted by this study.

Rates of Carbon Deposition for Suntech A at Low Velocity

The carbon deposition rates and cumulative carbon deposit formed are plotted for Suntech A at low velocity in Fig. 18, and a comparison of the rates of carbon deposition for similar tests using Jet A and Suntech A is shown in Fig. 19. In general, the trends displayed in the data for Suntech A are similar to those exhibited by Jet A at comparable test conditions, except that the carbon deposition rates for Suntech A can be as high as a factor of ten greater than those for Jet A. Also, as for Jet A, the peak in the carbon deposition rates vs. temperature curve occurs at about 560 K for tests lasting between 3 and 21 hr and having wall temperatures ranging from 500 to 625 K (i.e., maximum exit fuel temperature 505 to 560 K).

Rates of Carbon Deposition at High Velocity

The deposit data for the high velocity (1.3 m/s) and short duration tests using Jet A is plotted in Fig. 20. Because of the nonmonotonic heated-tube

wall temperature profiles caused by tube entrance effects which results in two different tube positions having the identical wall temperature (see Fig. 20a), the deposit rate and cumulative carbon deposit data are plotted as a function of tube position to permit differentiation of upstream and downstream temperatures. Isothermal tube data are also plotted for tube positions between 96 and 120 cm. In Fig. 20b, deposit rates are monotonically increasing with tube position in the regions of monotonically increasing wall temperature which suggests that depletion of active oxygenated species does not occur when the fuel residence time in heating is short (less than 1 s at this velocity condition). In fact, the magnitude of the deposit rates in Fig. 20b at high velocity are similar to those at the low velocity condition shown earlier in Fig. 13a at the common test condition of an initial wall temperature of 550 K (rates approximately equal to 150 $\mu g/cm^2$-hr). However, in the high velocity runs at wall temperatures greater than 550 K and for tube positions downstream of 60 cm, deposit rates are higher than those for the low velocity test at comparable wall temperatures. This comparison between the low and high velocity deposition data at similar wall temperatures reinforces the importance of the fuel temperature-time history in affecting downstream deposition, and the need to interpret deposit data considering this effect.

Fuel Oxidation and Deposition Model

The detailed chemical reactions that result in fuel deposits are very complex and not well understood at present. It is widely agreed, however, that at temperatures up to about 540 K (the principal region of interest in this investigation), they usually begin with a liquid phase oxidation of the fuel, which is promoted by dissolved oxygen. The fuel/oxygen reaction, which involves free radical chains is termed autoxidation. Common impurities such as compounds of sulfur, nitrogen, and metals enter and accelerate the reactions. Above 750 K, the deposition reaction is characterized by the pyrolysis of hydrocarbon molecules and the scission of hydrogen. Also, experimental trends indicate that the rate of deposit formation on heated surfaces is primarily affected by the local temperature and that the deposit forming mechanisms tend to be limited by the chemical kinetics of the deposition reaction rather than by diffusion.

Hazlett has identified the important deposit forming precursor species in his studies of reactions of aerated n-dodecane flowing over heated stainless steel tubes (Ref. 13). Using gas chromatography, he chemically analyzed the stressed fuel sample discharged from a JFTOT. Some results are shown in Fig. 21 where the concentrations of oxygenated species (hydroperoxides, alcohols, ketones, and carbon monoxide) are related to a light reflectance measurement of the deposit formed on the tube known as the tube deposit rating (ΔTDR). The data of Fig. 21 suggest that deposit formation (as characterized by ΔTDR) is closely related to the formation of oxygenated intermediary

precursor species. Further, researchers have established the following chain reaction mechanism to explain this trend (Ref. 1):

$$\text{Initiation} \qquad 2\ \text{R-H} + O_2 \xrightarrow{\text{Surface}} 2\text{R}\bullet + H_2O_2 \tag{1-a}$$

$$\text{Propagation} \begin{cases} \text{R}\bullet + O_2 \rightarrow RO_2\bullet & (1\text{-b}) \\ RO_2\bullet + \text{R-H} \rightarrow \text{ROOH} + \text{R}\bullet & (1\text{-c}) \end{cases}$$

$$\text{Termination} \begin{cases} RO_2\bullet + RO_2\bullet \rightarrow \text{ketone} + \text{alcohol} + O_2 & (1\text{-d}) \\ RO_2\bullet + \text{R}\bullet \rightarrow \text{ROOR} & (1\text{-e}) \\ \text{R}\bullet + \text{R}\bullet \rightarrow \text{R-R} & (1\text{-f}) \end{cases}$$

Initiation occurs on the hot metal surface through the formation of alkyl free radical (R•), and the propagation steps form the initial stable product, a hydroperoxide. The reaction is terminated by step (1-d) in the case of a high dissolved oxygen concentration and by step (1-f) at low oxygen concentration.

Because of the difficulty in applying the detailed deposition mechanism cited in Eqs. (1-a) through (1-f) to a multicomponent fuel, it is reasonable to postulate the following global two-step kinetic reaction mechanism:

$$\text{fuel} + O_2 \xrightarrow{k_1} \text{fuel} + \text{precursor} \tag{2-a}$$

$$\text{fuel} + \text{precursor} \xrightarrow{k_2} \text{fuel} + \text{deposit} \tag{2-b}$$

From Eqs. (2-a) and (2-b), the time rates of change of the active species are given by

$$\frac{d[O_2]}{dt} = -k_1\,[\text{fuel}]\,[O_2] \tag{3-a}$$

$$\frac{d[\text{deposit}]}{dt} = k_2\,[\text{fuel}]\,[\text{precursor}] \qquad (3\text{-b})$$

and

$$\frac{d[\text{precursor}]}{dt} = -\left(\frac{d[O_2]}{dt} + \frac{d[\text{deposit}]}{dt}\right) \qquad (3\text{-c})$$

where the brackets [ ] denote concentration in moles/cc. Because the sum of the concentrations of the O_2, precursor, and deposit species is small (a few ppm with respect to the fuel), the fraction of the fuel converted to deposit is negligible and is treated as a constant in the system. Also, the specific reaction rate constants for Eqs. (3-a) to (3-c) takes the Arrhenius form

$$k_n \equiv A_n \exp(-E_n/RT) \quad \text{cc/mole-s} \qquad (4)$$

Equations (2-a) and (2-b) require that at any time during the reaction, the sum of the concentrations of oxygen, precursor, and deposit is constant and equal to the initial concentration of oxygen, $[O_2]_{init}$, provided the initial concentrations of the precursor and deposit species are zero. Also, the reaction mechanism adopted permits the total production of deposit to be as high as $[O_2]_{init}$, and because of this, the value of $[O_2]_{init}$ input to the model is chosen so that the predicted deposit matches experimental data. Of course, an upper limit on the $[O_2]_{init}$ is the equilibrium value of dissolved oxygen in fully air-saturated fuel (about 55 ppm by weight or 1.4×10^{-6} moles O_2/cc fuel).

The values of the pre-exponential constants and activation energies required in Eq. (4) for each reaction, were obtained by solving Eqs. (3-a) and (3-b) for the specific reaction rates k_1 and k_2, and plotting each against reciprocal temperature on semilogarithmic graph paper from which the average slope (E_n/R) and intercept (A_n) were determined. Values for the concentrations of the individual species were approximated using the data in Figs. 13 and 21.

The values of these parameters were then adjusted so that the model fit selected experimental data, and the final values are given in Table IV. The value of $[O_2]_{init}$ was determined to be approximately 16 percent of that for oxygen saturated fuel. Also, as shown in Table IV, because the deposit formation rate data is based on carbon mass rather than total mass, the molecular weight of deposit was assumed equal to that of carbon to permit a consistent comparison between the model predictions and the experiment.

Equations (3) and (4) were written in finite difference form and solved on a digital computer using both an implicit backward difference Euler technique and an explicit fourth-order Runge-Kutta procedure. Both solution algorithms produced results which were within a few percent. The resultant computer program was applied to the heated and isothermal tube experiment assuming at any point along either tube, the system is modelled as a well-stirred reactor maintained at the local tube temperature. The reactor volume equals the total volume of fuel passed through the tube during the test. The calculation proceeds by dividing the tube into finite increments and marching in time along the length of the tube, where the time increment is computed from the specified tube incremental length and the local fuel velocity obtained from Fig. 8. Thus, given the wall and fuel temperature profiles along the tube, the test duration, the fuel flow rate, the initial concentration of oxygen in the fuel ($[O_2]_{init}$), and the pre-exponential and activation energy constants of Table IV, the fuel oxidation and deposition model integrates Eqs. (3-a) to (3-c) to produce the concentrations (and total masses) of oxygen, precursor, and deposit along the tube.

Figure 22 summarizes some predicted and measured deposit species concentration profiles along the tube for Jet A where the low velocity high temperature condition data of Run A-L-550-20 were used to calibrate the reaction model. The total deposit produced for the low velocity high temperature condition does not increase significantly downstream of 70 cm (because of suspected oxygen depletion), and these data provide a convenient point for setting the value of $[O_2]_{init}$ for all further runs of the model. In Fig. 22 for the high temperature condition, the model predicts that the precursor concentration reaches a maximum value prior to significant depletion of oxygen, and during precursor formation, deposit concentration is nearly proportional to precursor concentration. However, once the oxygen concentration is significantly reduced, the previously formed precursor is converted to deposit. Further, when the model is applied to the low temperature condition (Run A-L-350-50), Fig. 22 shows that the total deposit formed under these conditions is limited by the maximum tube temperature rather than by the oxygen concentration.

The predictive capability of the fuel oxidation and deposition model for a range of temperature conditions and flow rates is demonstrated in Fig. 23 for several short and long duration tests at low velocity and in Fig. 24 for a high temperature, short duration test at high velocity. The predicted and experimentally determined rates of carbon deposition for heated tubes are plotted against initial wall temperature (Fig. 23) and tube position (Fig. 24). As shown by Figs. 23 and 24, the agreement between the model and the experiment is satisfactory for extreme ranges of flowrates and wall temperature and for test durations that do not exceed 103 hr. However, since the model does not account for the enhancement effect on deposit formation of

an increase in active surface area provided by extremely thick and cellular deposits, it does not match the experimental data for tests with durations longer than 103 hr. Because of the large differences between the wall and fuel temperatures in the inlet portion of the tube for the high velocity test (see Fig. 6), the predictions presented in Fig. 24 are based on a modified temperature profile comprising the average of the fuel and wall temperatures over the first 15 cm of the tube (inlet region) and the wall temperature for the remainder of the tube. Also, for this case, the model correctly predicts that the deposit rate increases for the region of tube between 40 and 80 cm, and it suggests that this is because the oxygen in the fuel is not significantly depleted during the relatively short time the fuel is in the tube (about 0.9 s).

Overall Deposition Rate Constant Correlation

The results of the fuel oxidation and deposition model shown previously in Fig. 22 indicate that for the case of sufficient dissolved oxygen in the fuel, the concentration of deposit is proportional to the concentration of precursor. This relationship between these two species in this regime suggests a possible correlation, and when applied in the form of Eq. (3-b) it can be expressed as an overall deposition rate constant defined as

$$k_{ov} \equiv \left(\frac{1}{\text{deposit mass}}\right) \frac{d(\text{deposit mass/area})}{dt} \quad , \ \mu g/cm^2\text{-}s/\mu g \qquad (5)$$

where the deposit mass indicated is the cumulative carbon deposit mass at any point in the tube (see Figs. 12, 13b, and 18b). The term d(deposit mass/area)/dt is the time rate of change of the deposit mass along the tube and is computed by multiplying the incremental change in deposit mass loading per unit area and per unit length at any tube position by the fuel velocity at that position. The overall deposition rate constant of Eq. (5) incorporates the effects of fuel temperature-time and deposit history along the tube within the cumulative deposit mass, and the local effects of temperature and velocity.

The computed overall deposition rate constants for the Jet A and Suntech A data presented earlier are plotted as a function of reciprocal initial tube temperature in Figs. 25 and 26 respectively. In each figure, only data for the heated and isothermal tubes from the monotonically increasing portion of the carbon deposition rate vs. temperature curve are included, i.e., no significant depletion of dissolved fuel oxygen. In Figs. 25 and 26, the data are grouped as either long duration (> 50 hr) or short duration (< 50 hr), and in some instances, the heated-tube data are distinguished from the isothermal-tube data. Also, data from individual tests are identified to show the generality of the correlation, and a least squares curve fit (correlation coefficient = 0.95) is provided for the data of Fig. 25a.

As seen in Fig. 25a, the overall deposition rate constant defined by Eq. (5) satisfactorily correlates the heated and isothermal tube data for short durations with the isothermal tube data for long durations for two values of fuel velocity (0.07 and 1.3 m/s) and for a range of surface temperatures (400 to 700 K). However, for the heated-tube data from long duration tests shown in Fig. 25b, the correlation does not entirely remove the effect of test duration. Nevertheless, the vertical spread in the reduced data of Fig. 25b are far less than for the composite carbon deposition rate plot presented earlier as Fig. 14. Also, in comparing Figs. 25b and 26b, the overall deposition rate constants for Jet A and Suntech A at long and short durations are nearly the same, whereas their rates of carbon deposition were shown earlier to be different by a factor of ten (see Fig. 19). The information presented in Figs. 25 and 26 forms a basis for the development of a design/application procedure for analyzing deposit formation in fuel systems, and it identifies the surface temperature and temperature-time history of the fuel participating in the deposition reaction as two important parameters affecting deposit production.

CONCLUSIONS

1. Local deposit formation is primarily a function of local surface temperature, but fuel temperature-time history can have a significant effect.

2. The rates of carbon deposition are similar at low (0.07 m/s) and high (1.3 m/s) velocity, but deposit density varies by a factor of ten for these extremes.

3. The time-average rates of carbon deposition for deposits which are cellular in structure are not constant and increase with the second power of test duration. The increase is probably due to the additional surface area provided by the deposit.

4. A two-step kinetic model has been used to model the fuel oxidation and deposit formation process, and to correlate deposit formation as a function of test time, surface temperature, and fuel temperature-time history.

REFERENCES

1. ANON: CRC Literature Survey on the Thermal Oxidation Stability of Jet Fuel. CRC Report No. 590, Coordinating Research Council, Inc., Atlanta, GA., April 1979.

2. Szetela, E. J.: Deposits from Heated Gas Turbine Fuels. ASME Paper No. 76-GT-9, 1976.

3. Hatcher, J. B.: High-Flux Heat Transfer and Coke Deposition of JP3 Fuel Mixture, JPL CIT Progress Report No. 20-157, February 1952.

4. Mills, J. S. and F. R. Edwards: The Thermal Stability of Aviation Fuel, ASME 84-GT-69, 1984.

5. Watt, J. J., A. Evans, and R. R. Hibbard: Fouling Characteristics of ASTM Jet-A Fuel When Heated to 700 F in a Simulated Heat Exchanger Tube, NASA TN D-4958, December 1968.

6. Taylor, W. F.: Development of High Stability Fuel, Exxon Report GRUS, 11GAHF.73, July 1973.

7. Szetela, E. J. and J. A. TeVelde: Experimental Study of External Fuel Vaporization, Combustion Science and Technology, V. 35, 1983.

8. Roback, R., E. J. Szetela, and L. J. Spadaccini: Deposit Formation in Hydrocarbon Fuels, ASME J. Engineering for Power, V. 105, 1983.

9. TeVelde, J. A., L. J. Spadaccini, E. J. Szetela, and M. K. Glickstein: Alternative Fuel Deposit Formation, AGARD CP-353, 1983.

10. Peat, A. E.: Thermal Decomposition of Aviation Fuel, ASME 82-GT-27, 1982.

11. Bradley, R., R. Bankhead, and W. Bucher: High Temperature Hydrocarbon Fuels Research in an Advanced Aircraft Fuel System Simulator, AFFB-14-70, AFAPL-TR-73-95, April 1974.

12. Faith, L. E., G. H. Ackerman, and H. T. Henderson: Heat Sink Capability of Jet A Fuel: Heat Transfer and Coking Studies, NASA CR-72951, July, 1971.

13. Hazlett, R. N.: Progress Report on Advanced Hydrocarbon Fuel Development, Naval Research Laboratory, March, 1975.

LIST OF SYMBOLS

A	experimentally-determined reaction constant
C_p	specific heat at constant pressure
E	Arrhenius activation energy
k	thermal conductivity; specific rate constant
R	universal gas constant, 1.987 cal/g-mole-K
Re	Reynolds number based on tube diameter
T	temperature
t	time
μ	absolute viscosity
ρ	density

Subscripts

init	initial
n	reaction number
ov	overall
res	residence

Miscellaneous

[ ]	concentration, moles/cc

TABLE I

CERTIFIED FUEL ANALYSES

	Jet A	Suntech A
Specific gravity @ 289 K (ASTM D 1298)	0.8165	0.863
Viscosity, cSt (ASTM D 445)		
@ 311 K	1.51	1.99
@ 323 K	1.25	1.65
@ 328 K	1.18	1.54
@ 372 K	0.75	0.92
Distillation Temperatures, K (ASTM D 86)		
Initial Boiling Point	441	448
10% Recovery	461	469
20%	468	482
50%	486	514
90%	518	578
End Point	539	626
Paraffins, vol. % (ASTM D 1319)	76.84	59.47
Olefins, vol. % (ASTM D 1319)	1.95	0.75
Aromatics, vol. % (ASTM D 1319)	21.21	39.77
Sulfur, wt. % (ASTM D 2622)	0.051	0.237
Nitrogen, ppm by wt. (chemiluminescent)	12.4	249
Hydrogen, wt. % (Perkin-Elmer 240 Analyzer)	13.45	12.38
Organic Oxygen, wt. % (Perkin-Elmer 240 Analyzer)	0.56	1.42
Thermal Stability Breakpoint Temperature, K (JFTOT ASTM D 3241, visual code 3, ± 3 K)	525 to 533	538

TABLE II

APPROXIMATE THERMOPHYSICAL PROPERTIES OF JET A AND SUNTECH A*

T (F)	T (K)	ρ (kg/m^3)	C_p ($kJ/kg \cdot K$)	μ ($kg/m \cdot s$) x 10^4	k ($W/m \cdot K$)
0	255	820	1.59	52.3	0.145
100	311	780	1.80	13.9	0.137
200	366	740	2.10	6.42	0.130
300	422	697	2.37	3.92	0.121
400	478	657	2.62	2.75	0.114
500	533	612	2.69	1.99	0.107
600	589	556	2.93	1.46	0.0986
800	700	352	4.45	0.358	0.0554
1000	811	136	3.04	0.135	0.0312

* All properties evaluated at 3.65 MPa

TABLE III-A

SUMMARY OF TEST CONDITIONS FOR JET A[1]

Run No.	Test Ident. Code[2]	Inlet Velocity (m/s)	Duration (hr)	Nominal Fuel Outlet Temp. (K)	Max. Tube Wall Temp. (K)
1	A-L-550-4	0.07	3.7	555	621
2	A-L-550-7		6.7	560	619
3	A-L-550-10		10.4	560	618
4	A-L-450-10		10.4	505	564
5	A-L-550-20/1		20.0	560	609
6	A-L-550-20/2		20.0	560	629
7	A-L-550-20/3		20.0	560	630
8	A-L-350-50		50.0	450	500
9	A-L-350-53		52.6	450	506
10	A-L-350-103		102.7	455	507
11	A-L-350-157/1[3]		157.1	465	508
12	A-L-350-157/2[3]		157.1	450	514
13	A-L-300-169		169.0	420	472
14	A-L-300-233		233.2	420	473
15	A-L-300-406		406.3	420	467
16	A-L-300-639[3]		639.5	420	467
17	A-L-300-730[3]		730.3	430	465
18	A-H-420-21/1	1.3	21.4	490	735
19	A-H-420-21/2		21.4	490	729
20	A-H-450-21		21.4	505	762

(1) All tests run at a nominal inlet fuel pressure and temperature of 3.4 MPa and 290 K, respectively

(2) Key to test identification
x-y-zzz-www/u

where x - Fuel type; A=Jet A; S=Suntech A
y - Tube inlet velocity; L=0.07 m/s; H=1.3 m/s
zzz - Maximum fuel temp. in (F)
www - Test duration in (hr)
u - Counter index for repeat tests

(3) Tube plugged

TABLE III-B

SUMMARY OF TEST CONDITIONS FOR SUNTECH A[1]

Run No.	Test Ident. Code[2]	Inlet Velocity (m/s)	Duration (hr)	Nominal Fuel Outlet Temp. (K)	Max. Tube Wall Temp. (K)
1	S-L-550-3	0.07	3.3	560	629
2	S-L-450-10		9.5	505	575
3	S-L-450-11		11.2	505	556
4	S-L-550-17		17.4	560	626
5	S-L-550-21		20.7	560	624
6	S-L-300-23		22.6	420	486
7	S-L-300-190		189.9	435	487
8	S-L-300-213[3]		212.6	420	489
9	S-L-300-213[3]		212.6	420	485

(1) All tests run at a nominal inlet fuel pressure and temperature of 3.4 MPa and 290 K, respectively

(2) Key to test identification
x-y-zzz-www/u

where x - Fuel type; A=Jet A; S=Suntech A
y - Tube inlet velocity; L=0.07 m/s; H=1.3 m/s
zzz - Maximum fuel temp. in (F)
www - Test duration in (hr)
u - Counter index for repeat tests

(3) Tube plugged

TABLE IV

FUEL OXIDATION AND DEPOSITION MODEL PARAMETERS

Reaction Equation	A_n (cc/mole-s)	E_n (kcal/mole)
2-a	3.5×10^9	17
2-b	2.0×10^{14}	31

$[O_2]_{init} = 2.25 \times 10^{-7}$ moles/cc
Molecular weight of deposit = 12 g/mole
Molecular weight of fuel = 170 g/mole

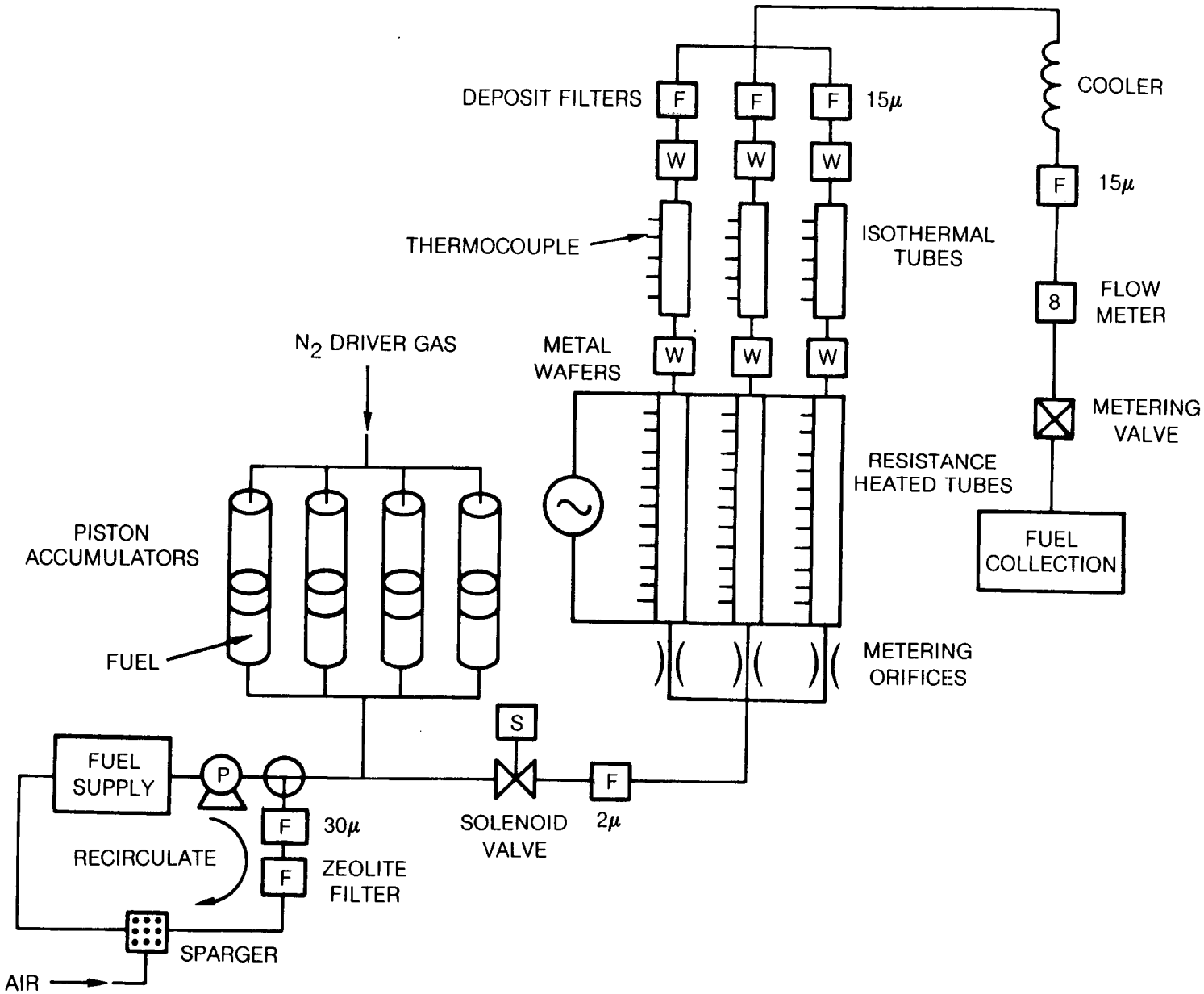

85-3-68-3

Figure 1. Fuel Deposit Test Apparatus

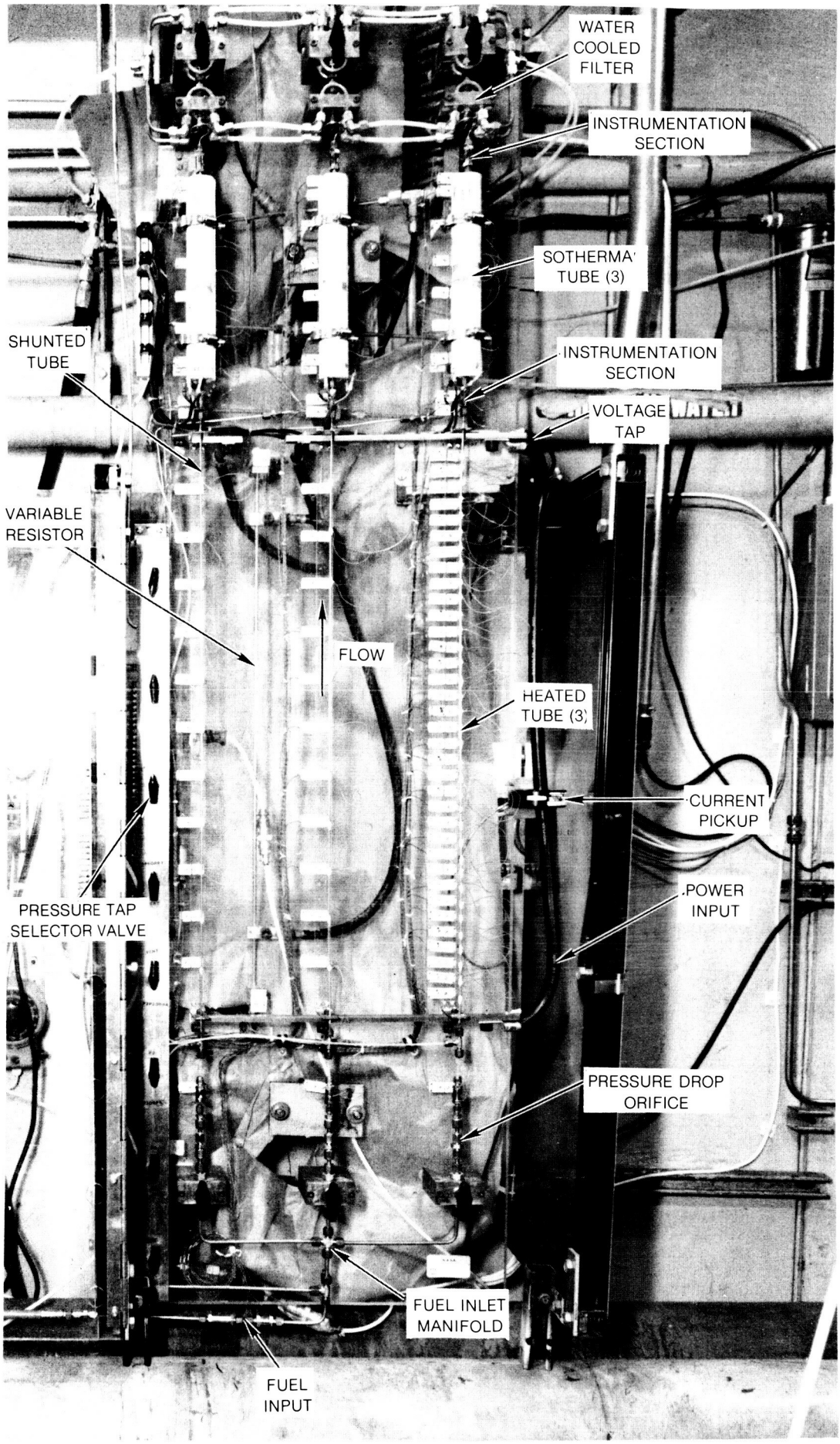

Figure 2. Test Tube Assembly

84–4–76–2

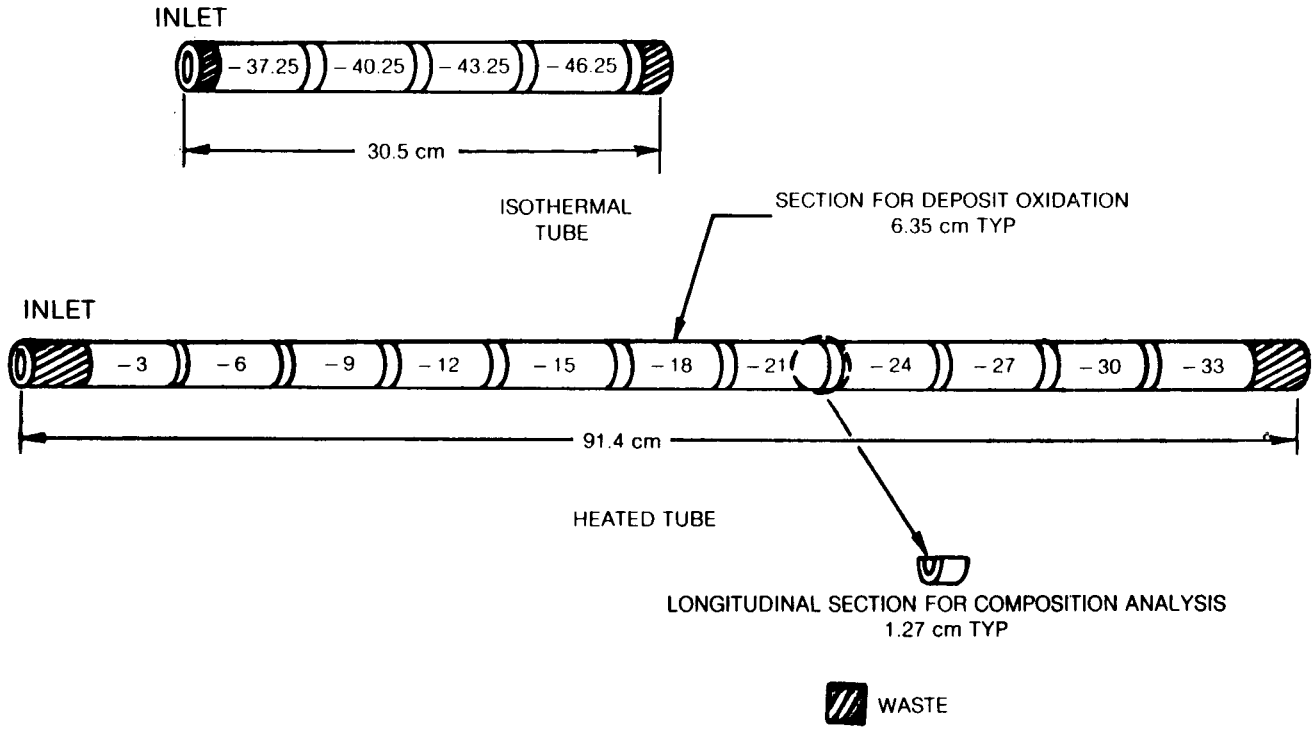

Figure 3. Tube Sectioning

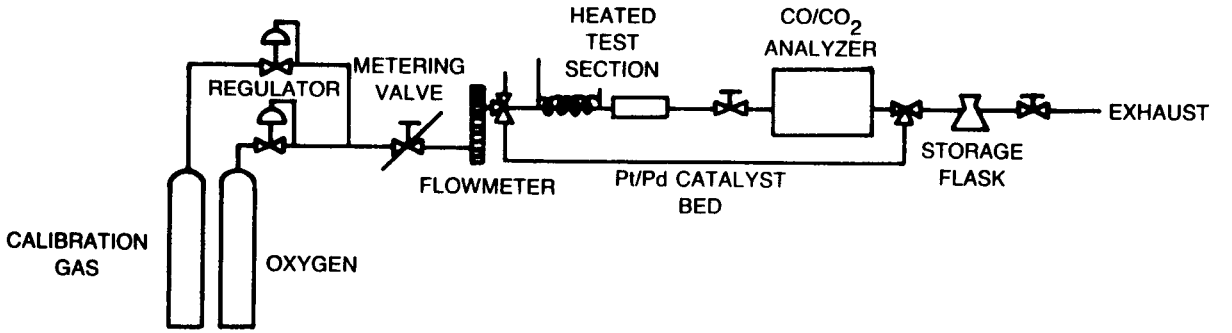

Figure 4. Deposit Oxidation Apparatus

87-4-39-1

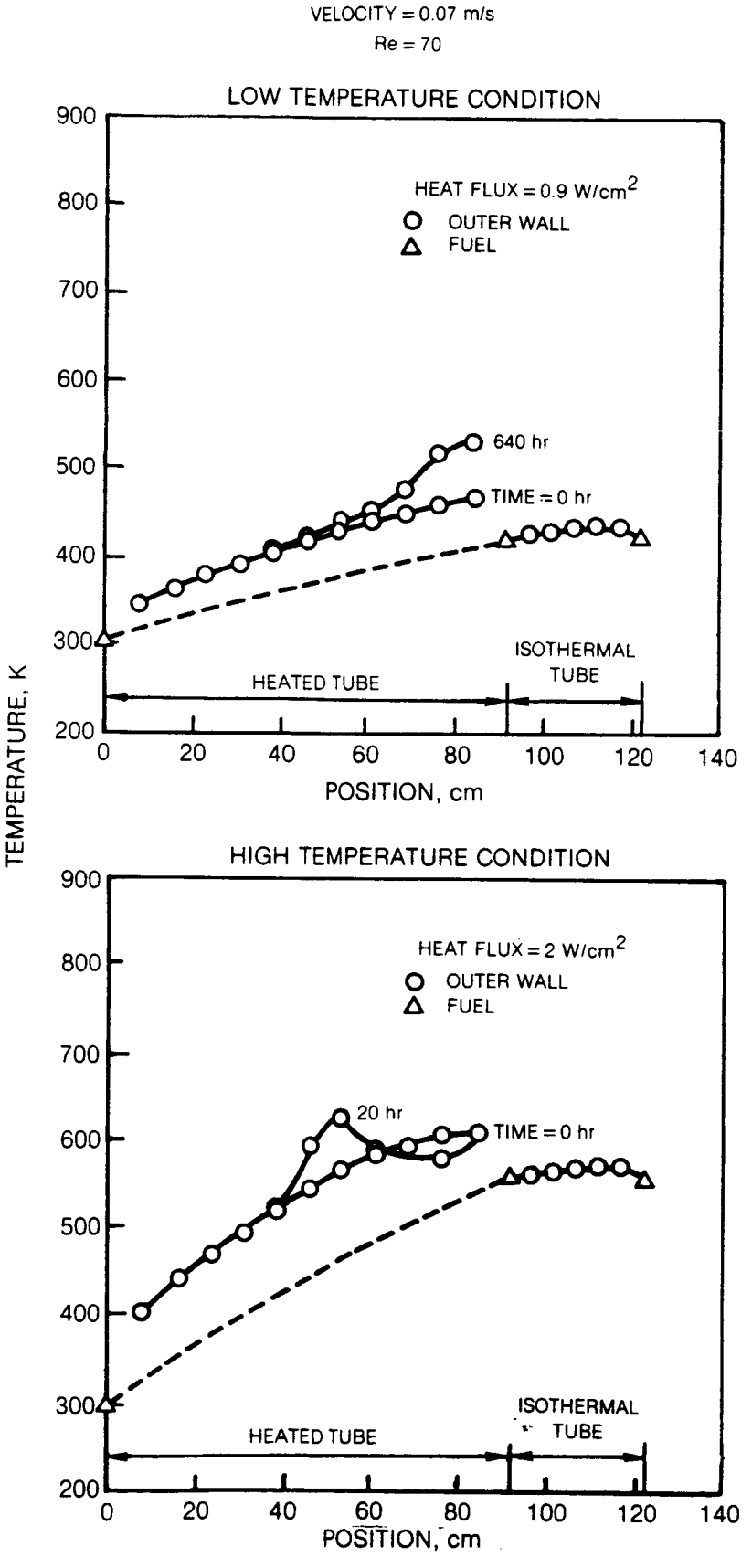

Figure 5. Wall and Fuel Temperature Distributions for Jet A at Low Velocity

85-3-68-5

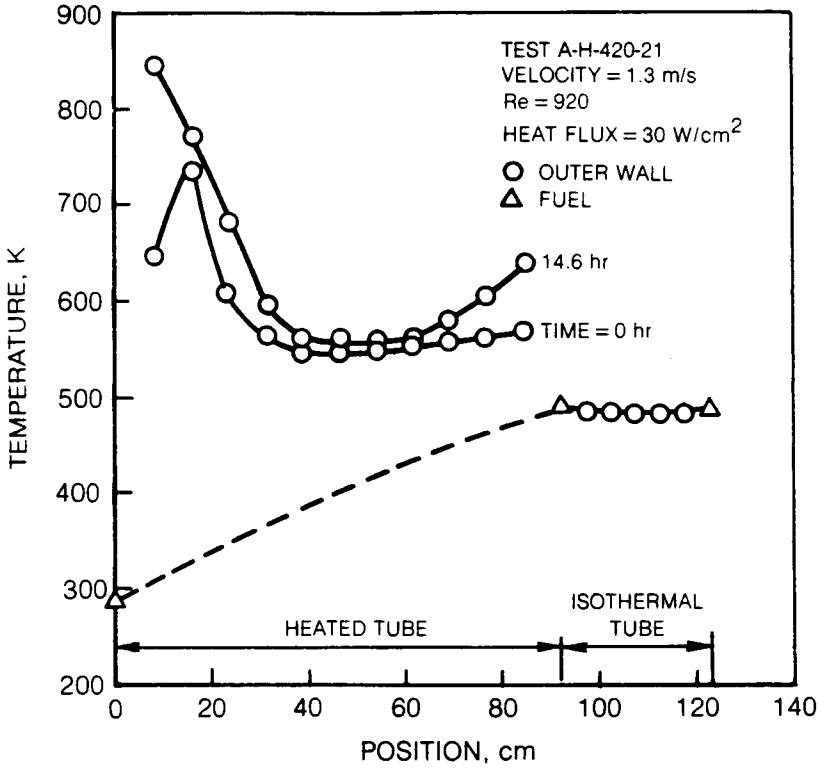

Figure 6. Wall and Fuel Temperature Distributions for Jet A at High Velocity

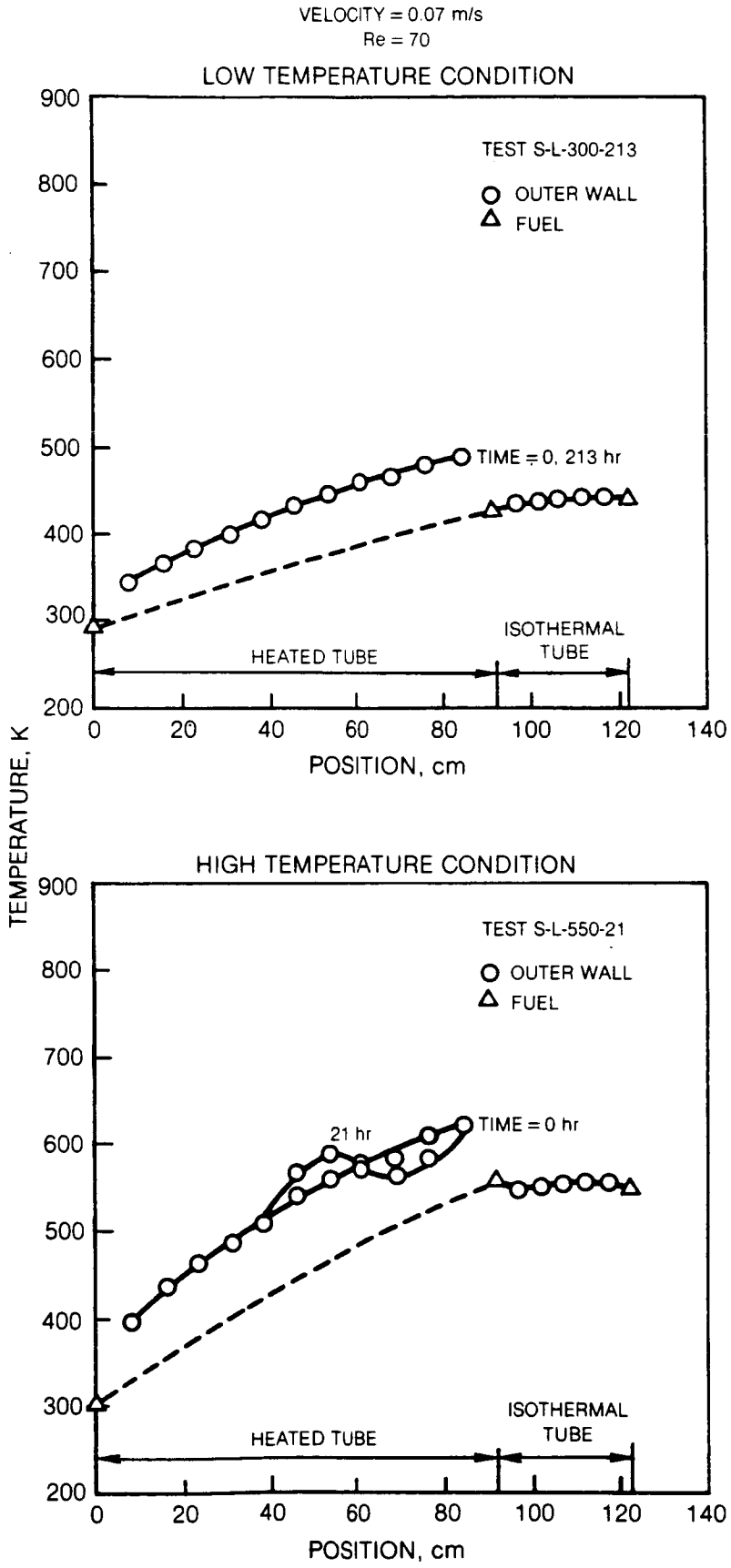

Figure 7. Wall and Fuel Temperature Distributions for Suntech A at Low Velocity

85-3-68-6

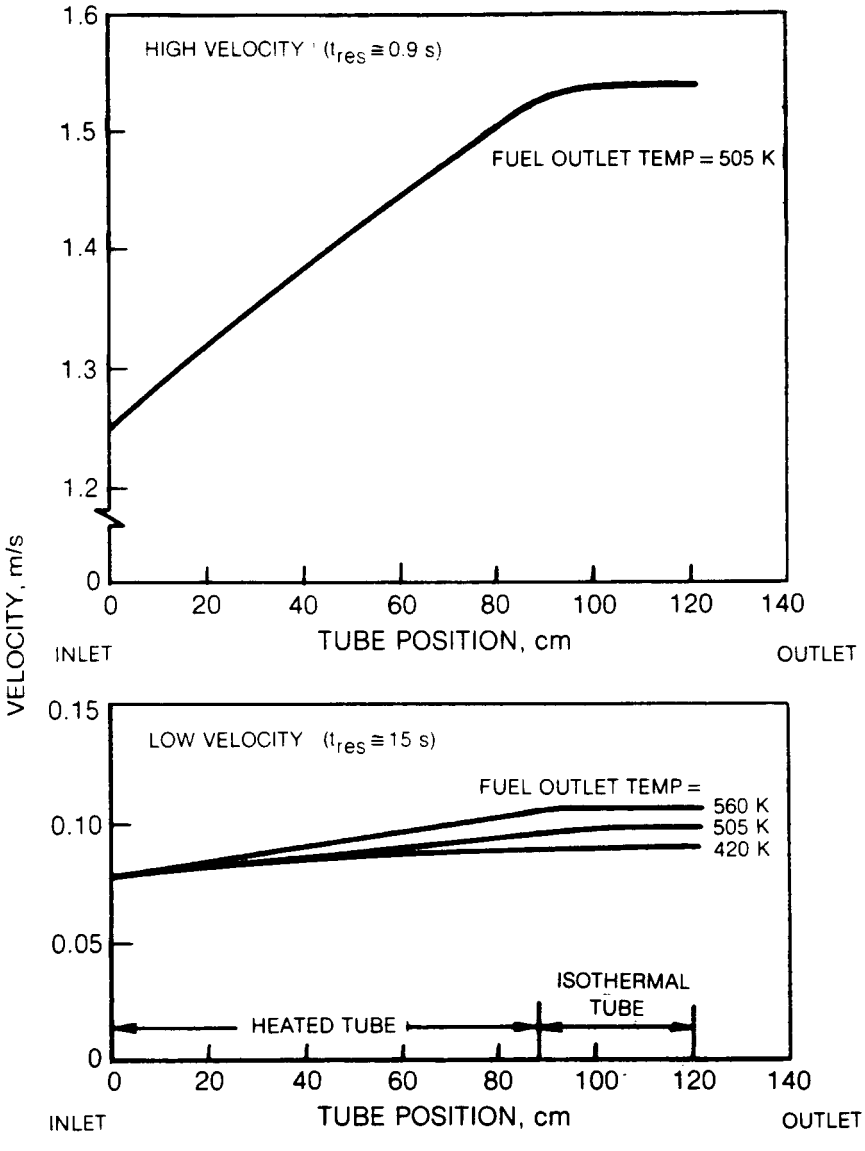

Figure 8. Mean Fuel Velocity Distributions Along the Tube

TUBE TEMPERATURE = 590 K
TEST DURATION = 20 hr

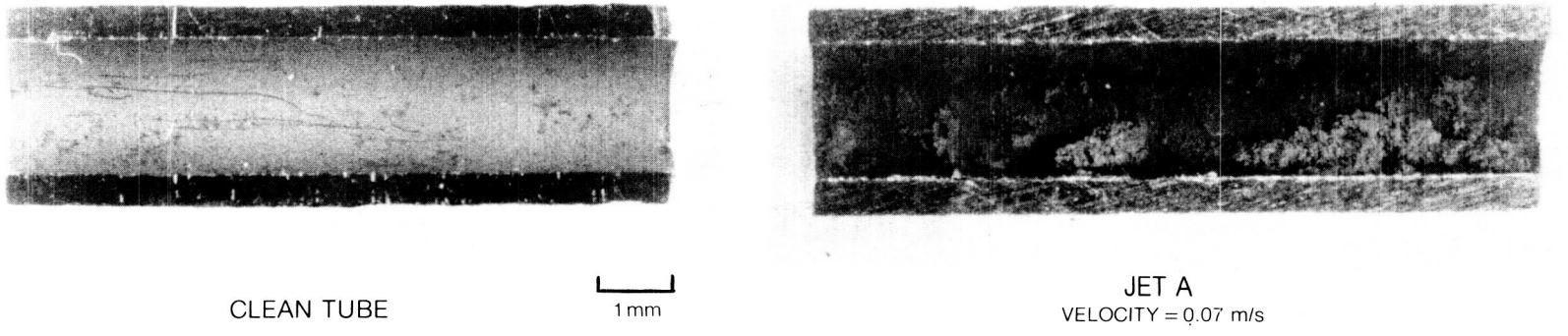

CLEAN TUBE

JET A
VELOCITY = 0.07 m/s

JET A
VELOCITY = 1.3 m/s

SUNTECH A
VELOCITY = 0.07 m/s

Figure 9. Fuel Deposits on a Heated 316-Stainless-Steel Tube

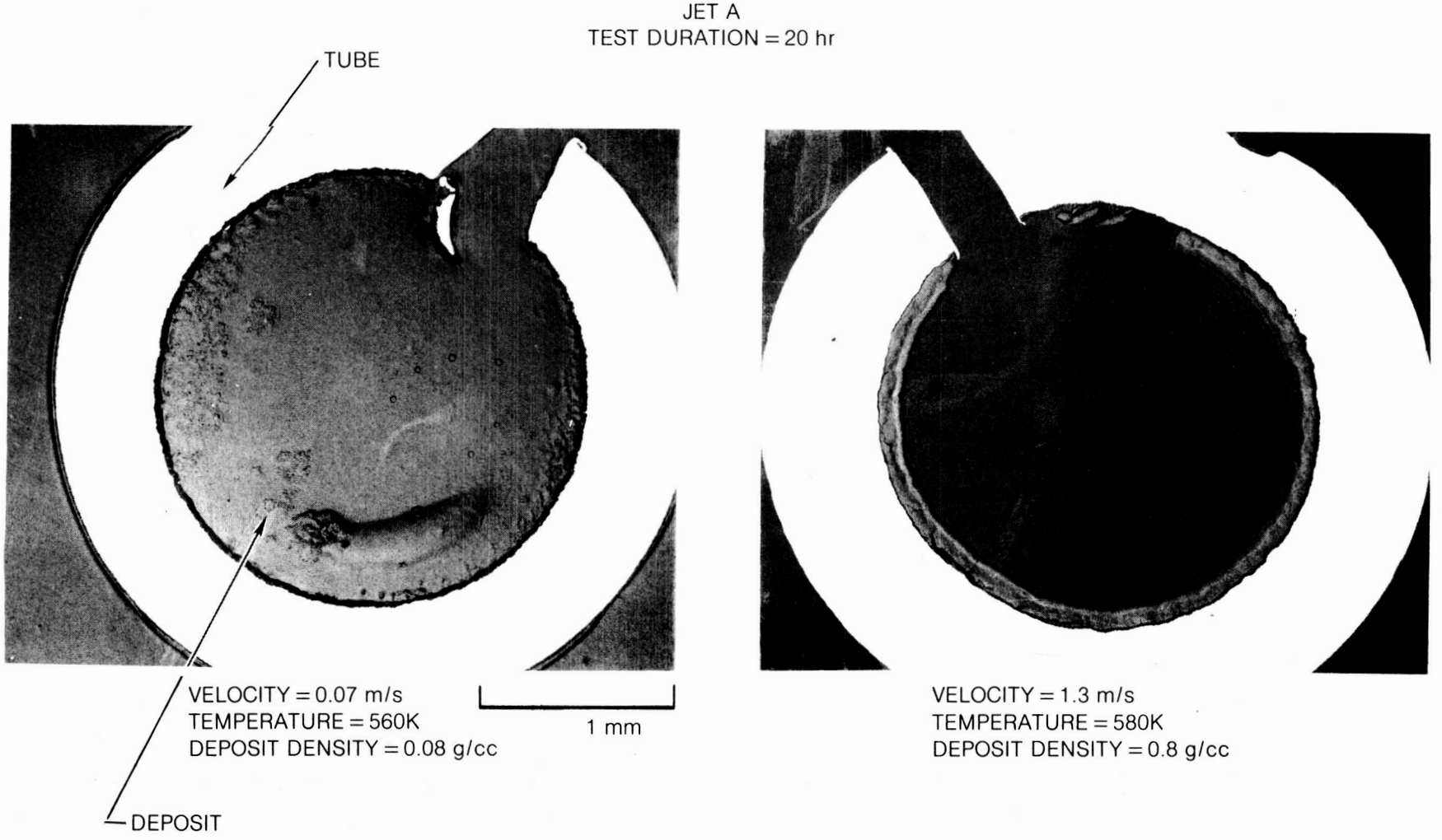

85-3-68-25

Figure 10. Effect of Fuel Velocity on Deposit Structure

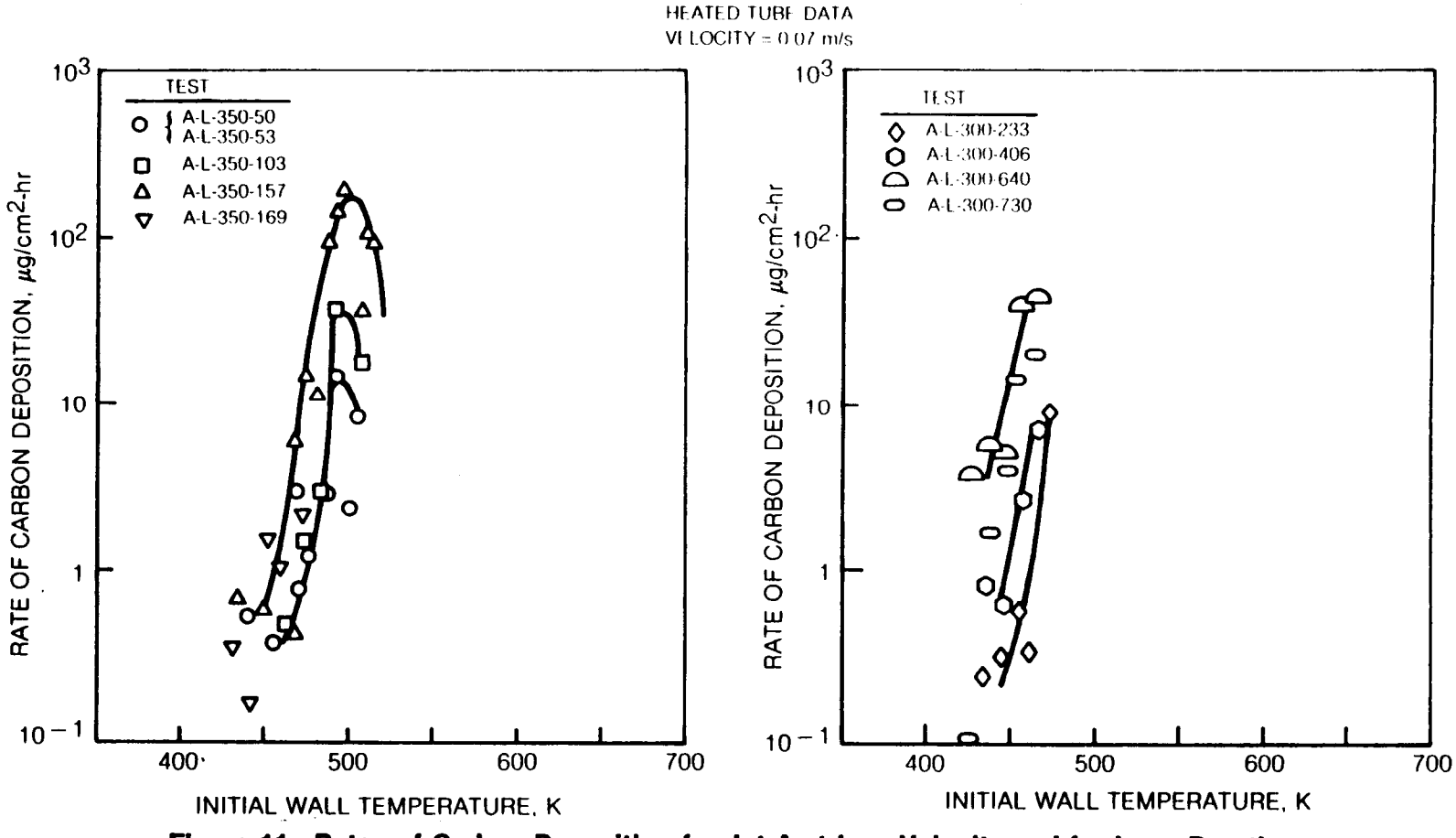

Figure 11. Rates of Carbon Deposition for Jet A at Low Velocity and for Long Duration

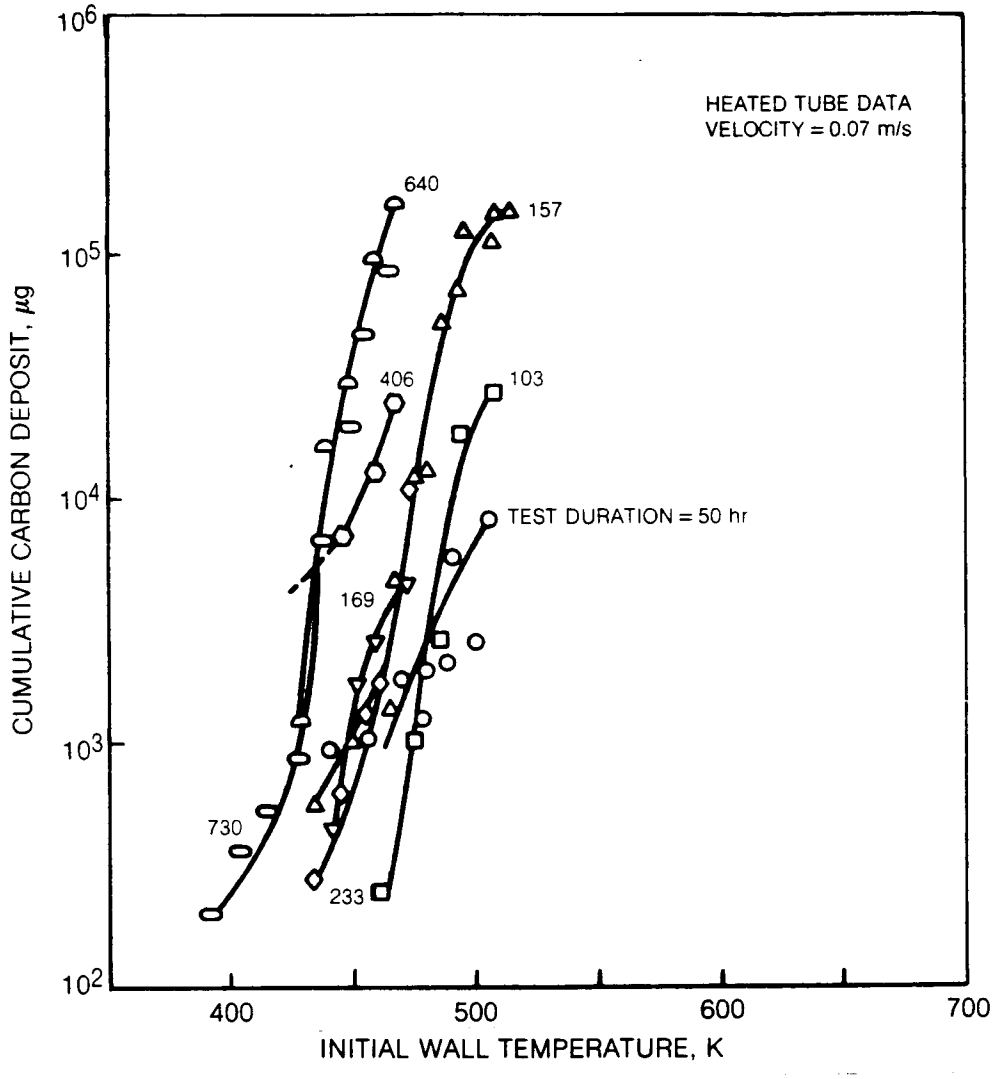

Figure 12. Cumulative Carbon Deposition for Jet A at Low Velocity and for Long Durations

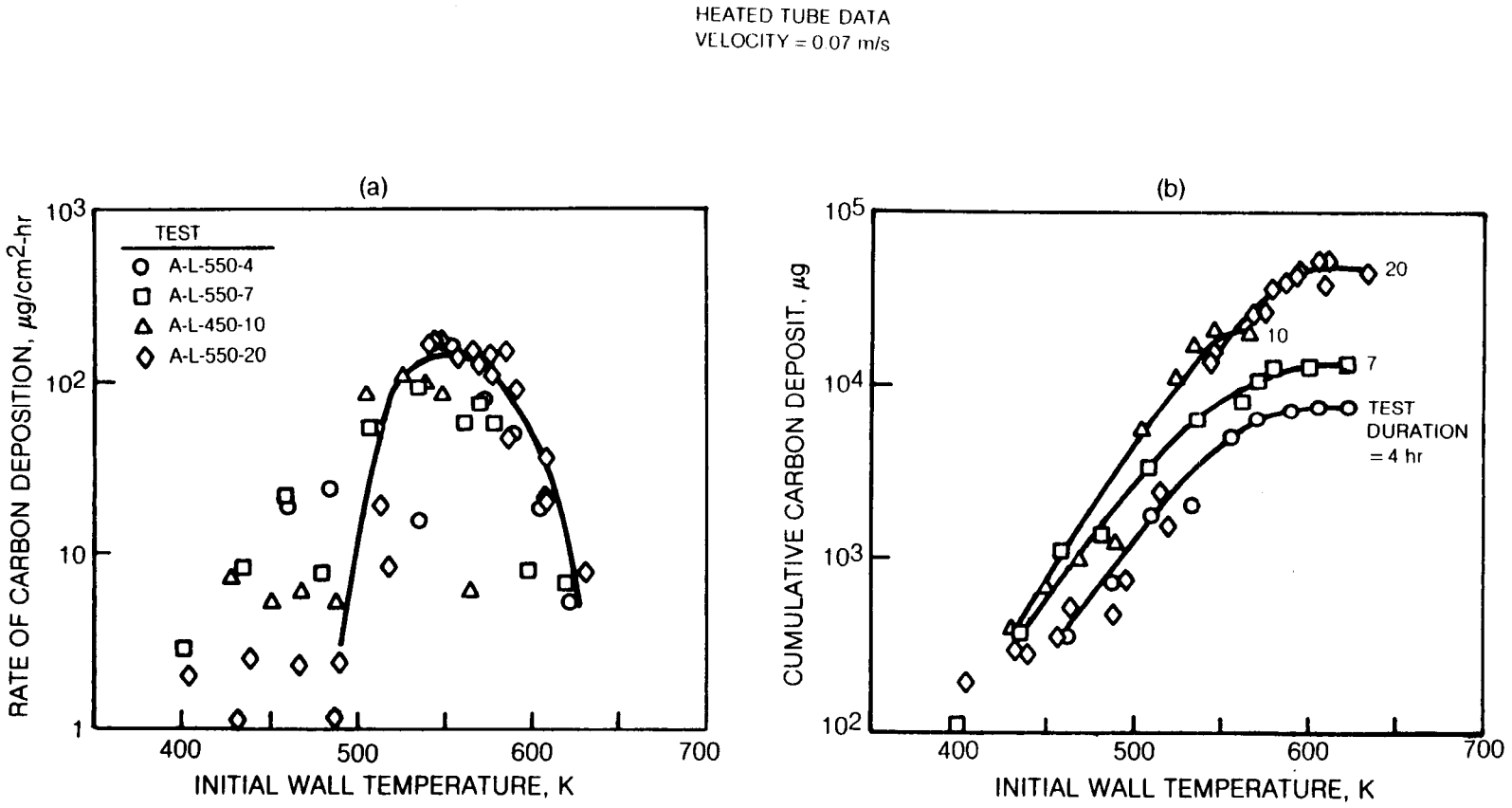

Figure 13. Carbon Deposition for Jet A at Low Velocity and for Short Durations

85-3-68-10

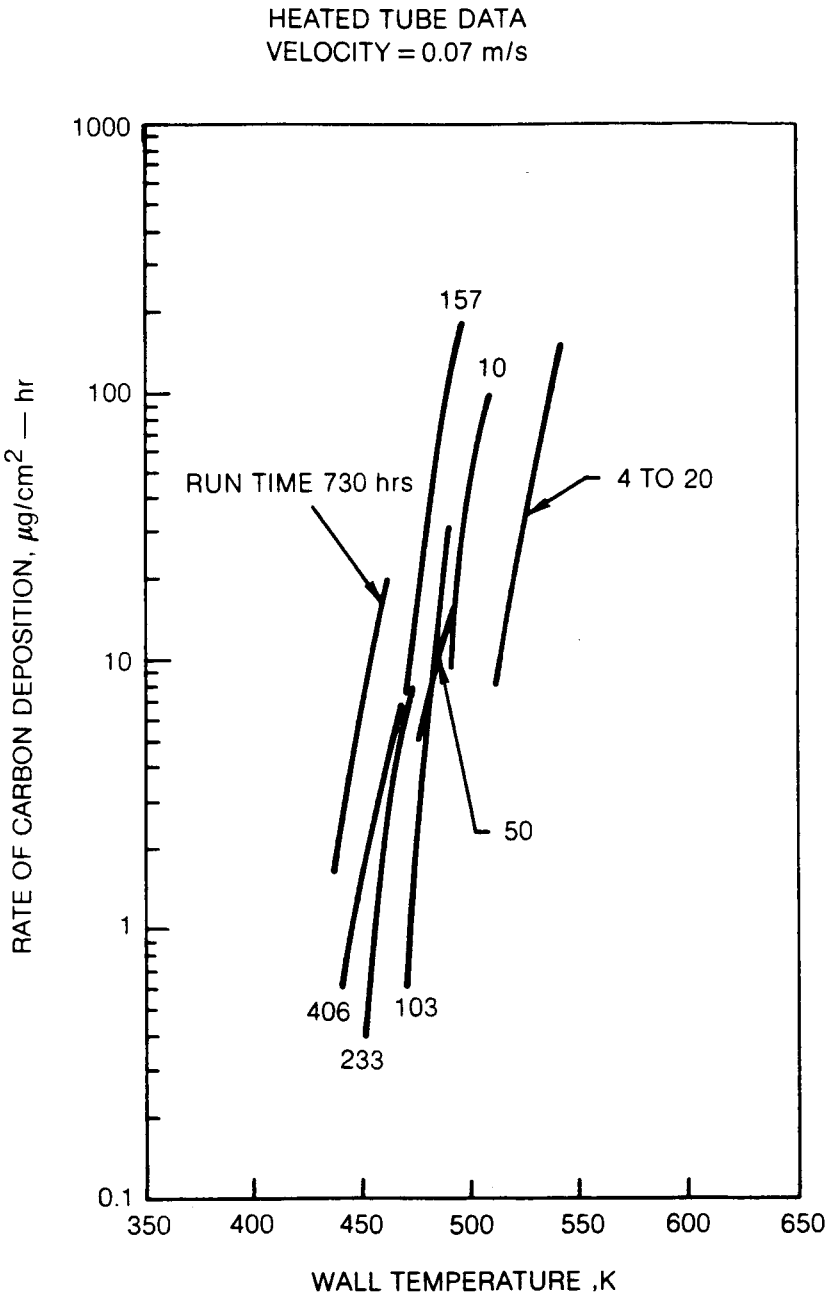

Figure 14. Effect of Test Duration on Carbon Deposition Rate for Jet A at Low Velocity

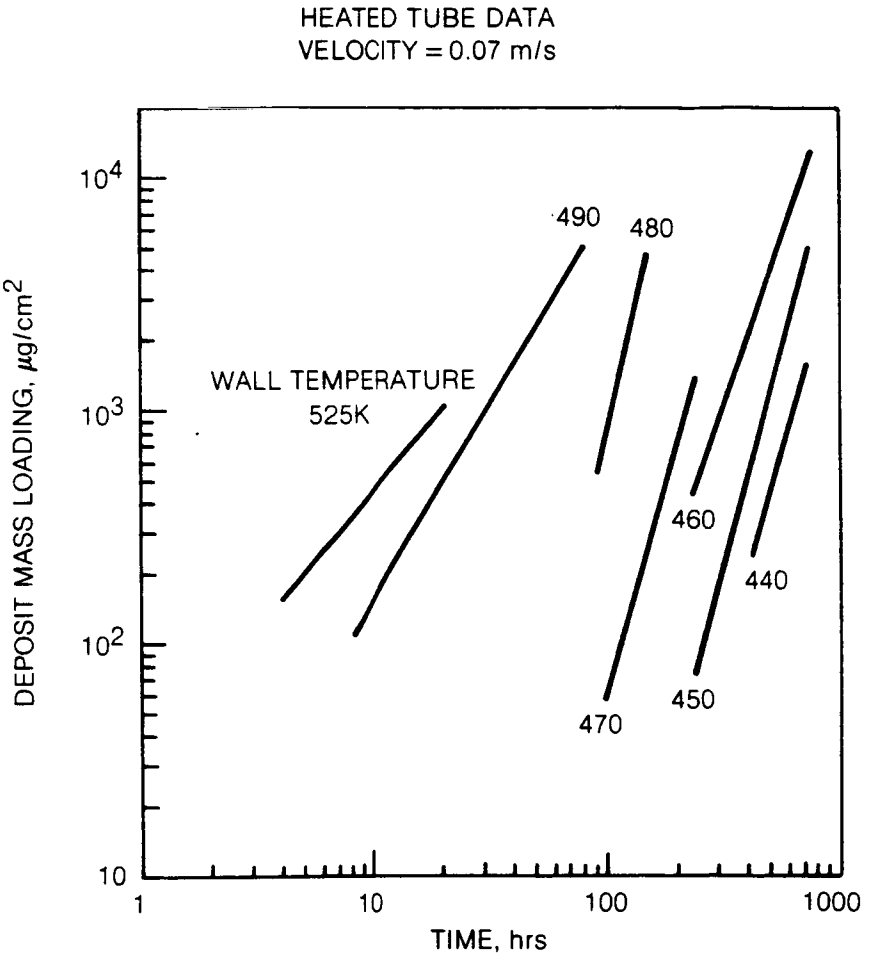

Figure 15. Increase of Carbon Loading With Time for Jet A at Low Velocity

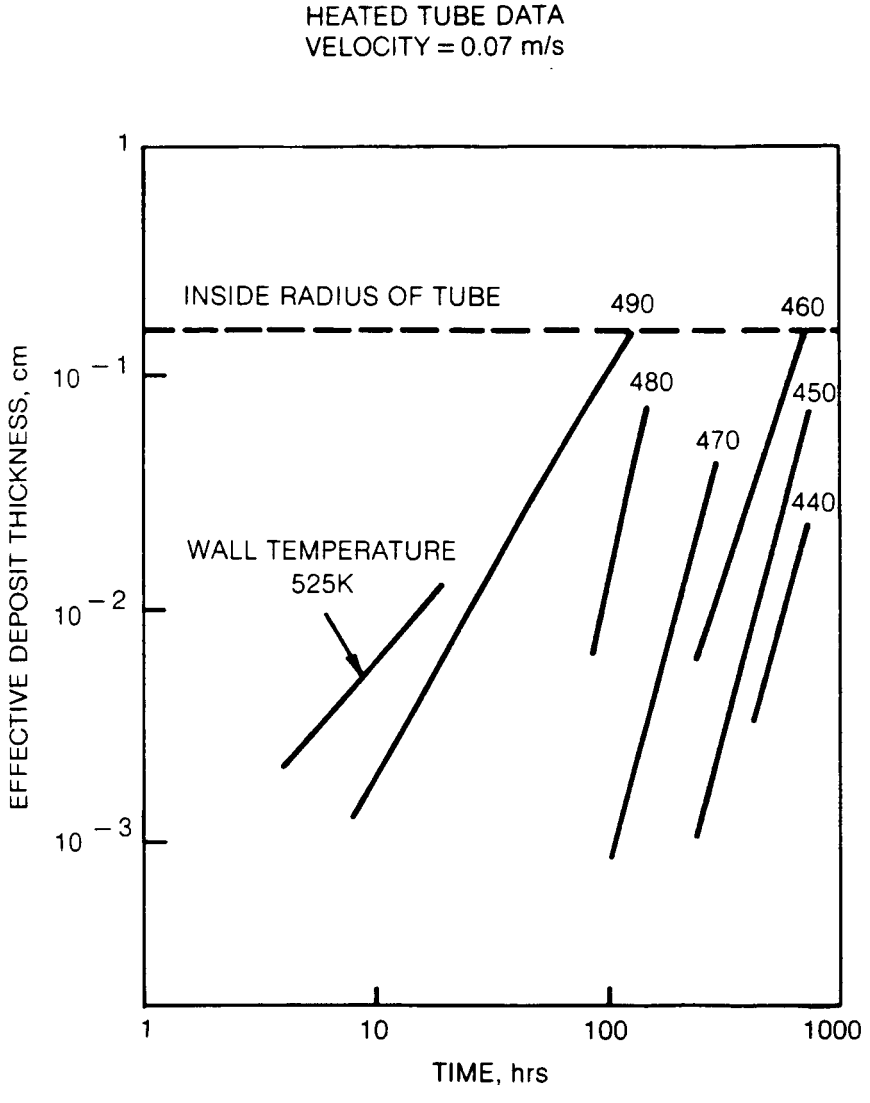

Figure 16. Increase of Deposit Thickness with Time for Jet A at Low Velocity

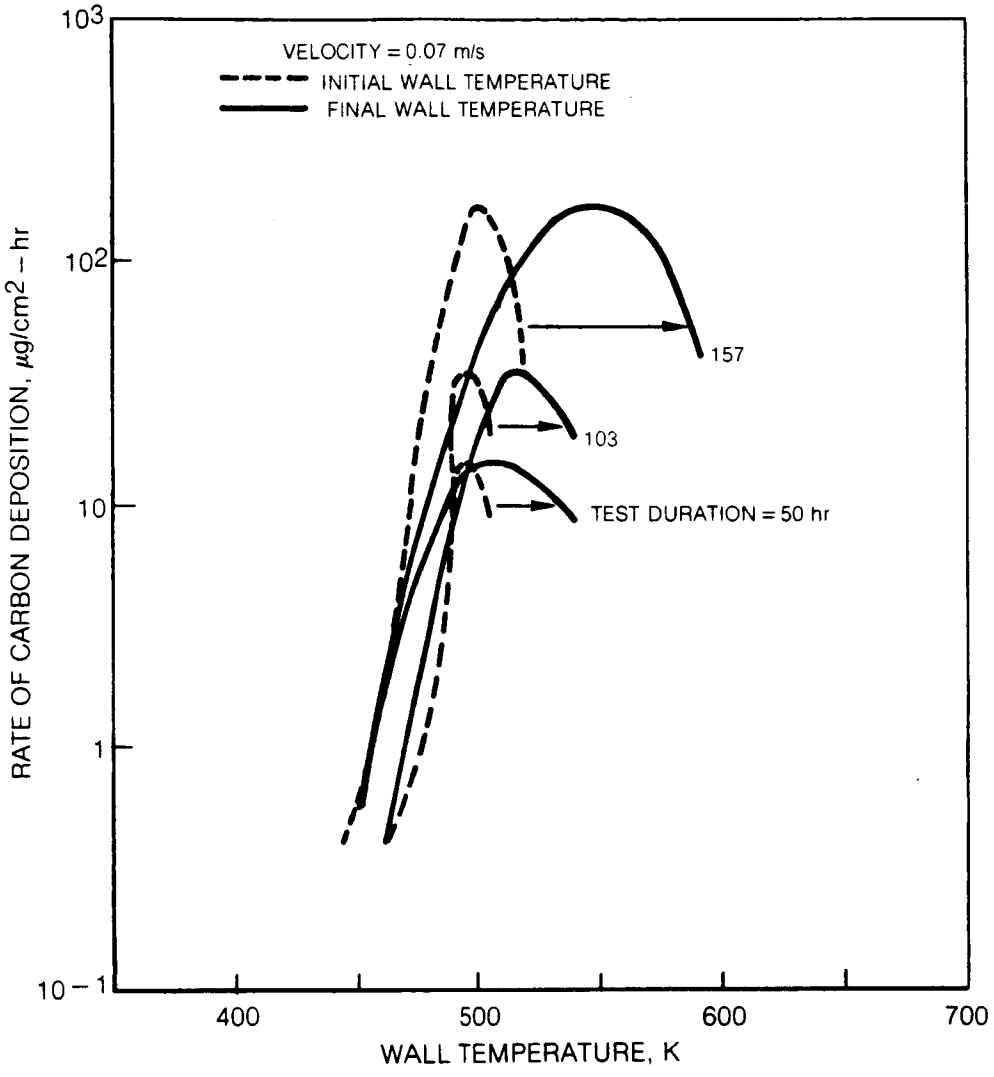

Figure 17. Effect of Correlation Temperature on the Rates of Carbon Deposition for Jet A

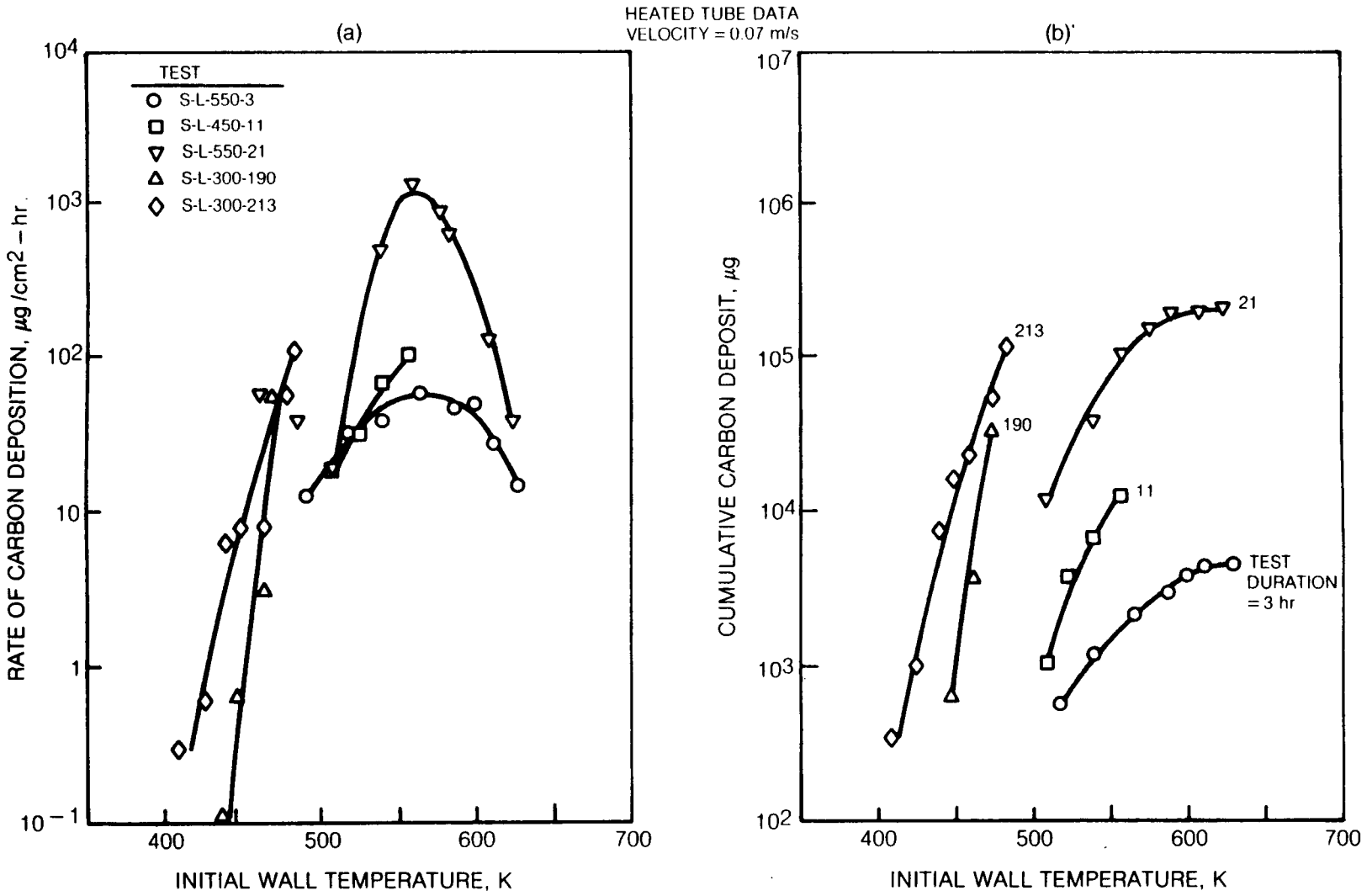

Figure 18. Carbon Deposition for Suntech A at Low Velocity

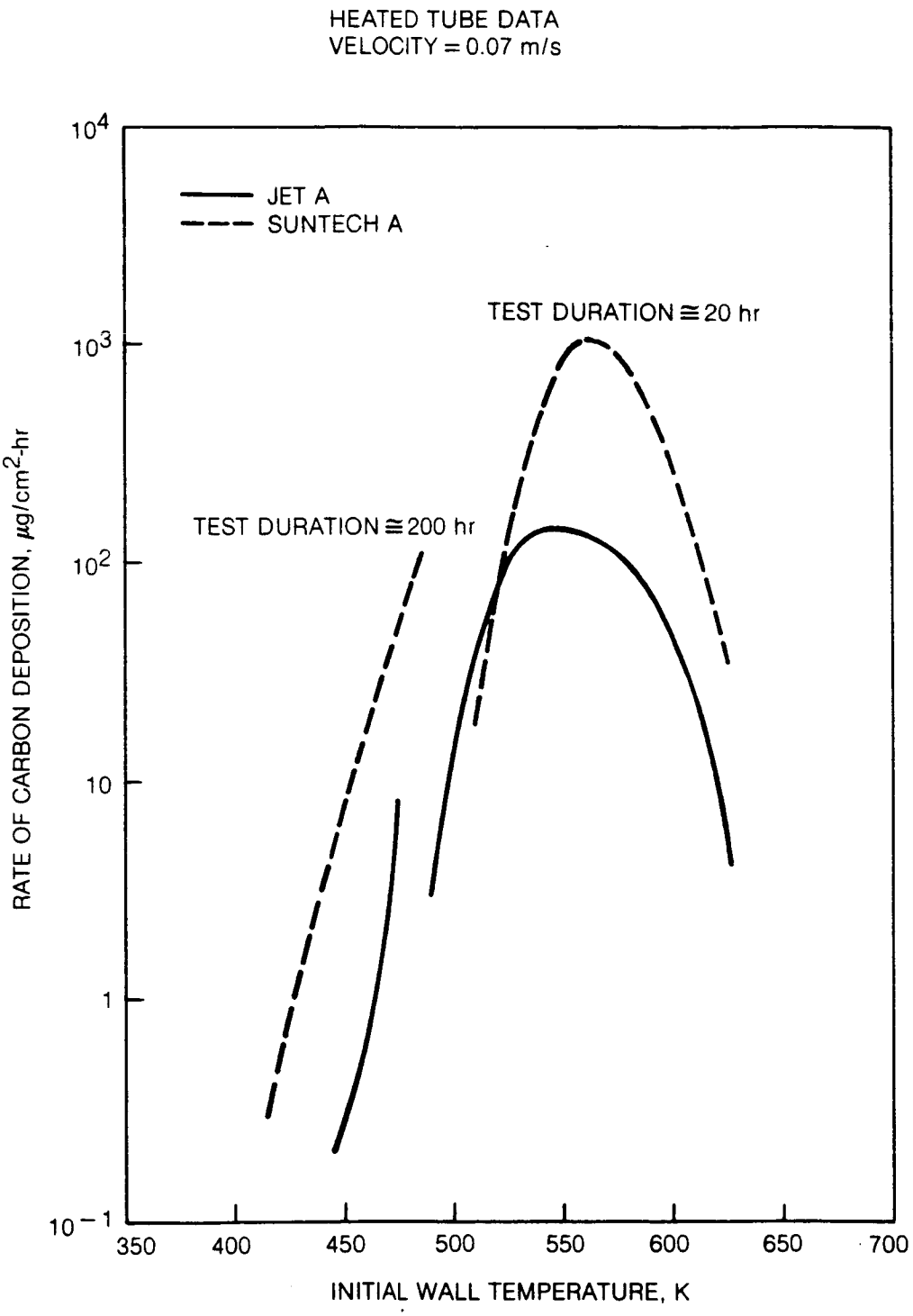

Figure 19. Comparison of the Rates of Carbon Deposition for Jet A and Suntech A at Low Velocity

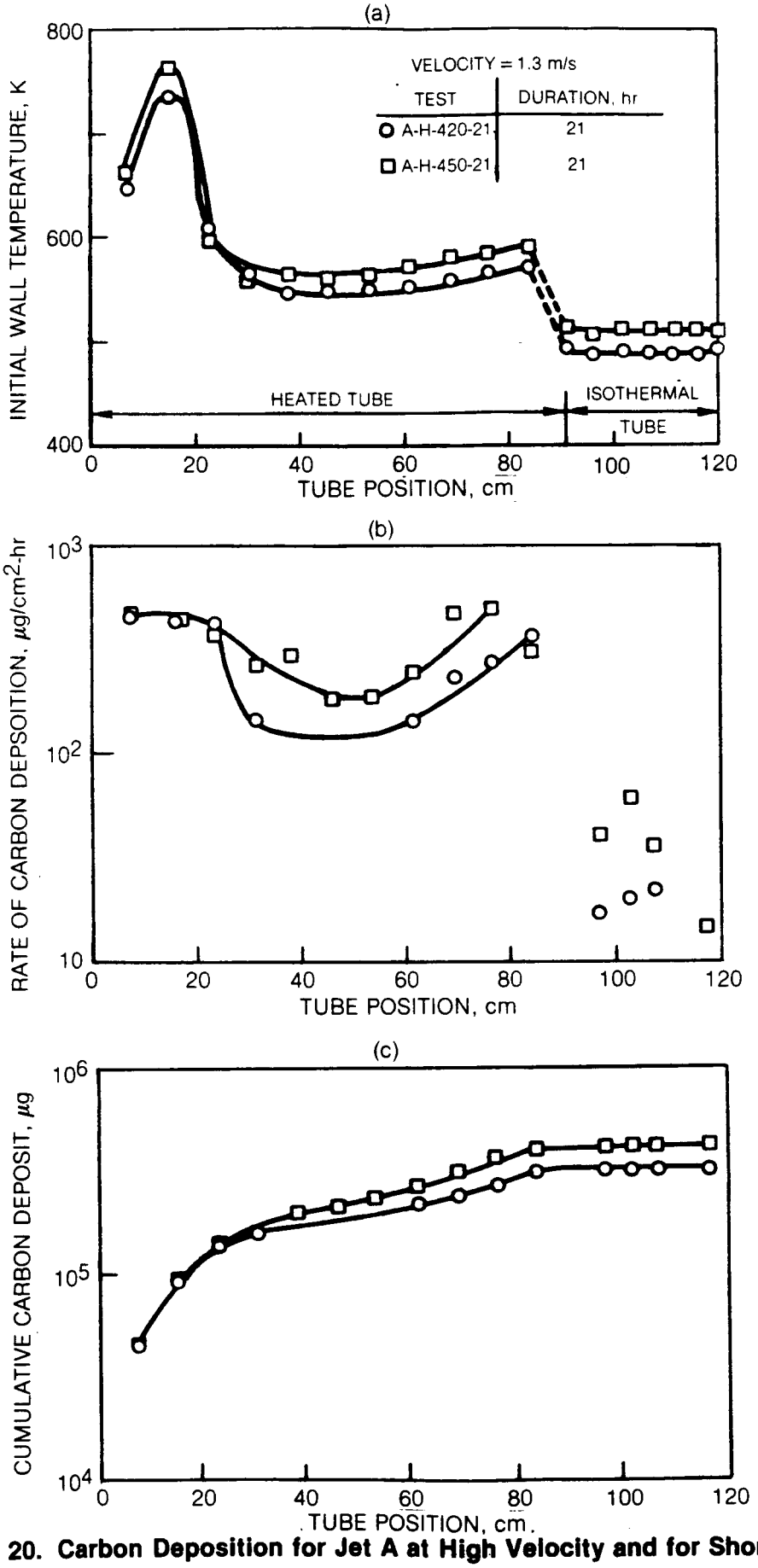

Figure 20. Carbon Deposition for Jet A at High Velocity and for Short Durations

85-3-68-8

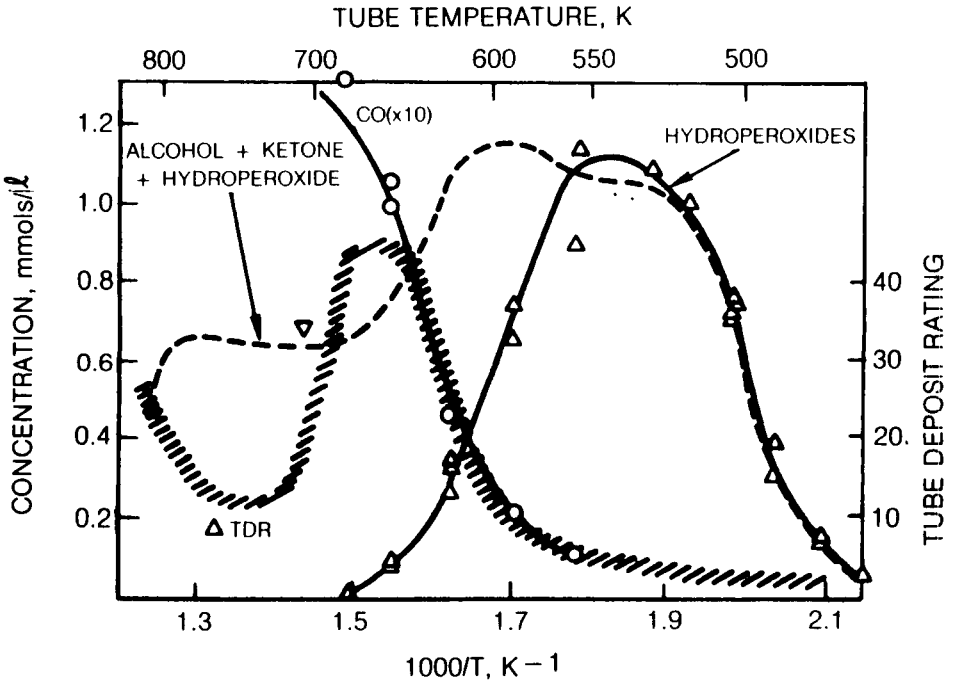

Figure 21. Oxygenated Compounds from n-Dodecane Flowing Over a 316-Stainless-Steel Tube (Ref. 13)

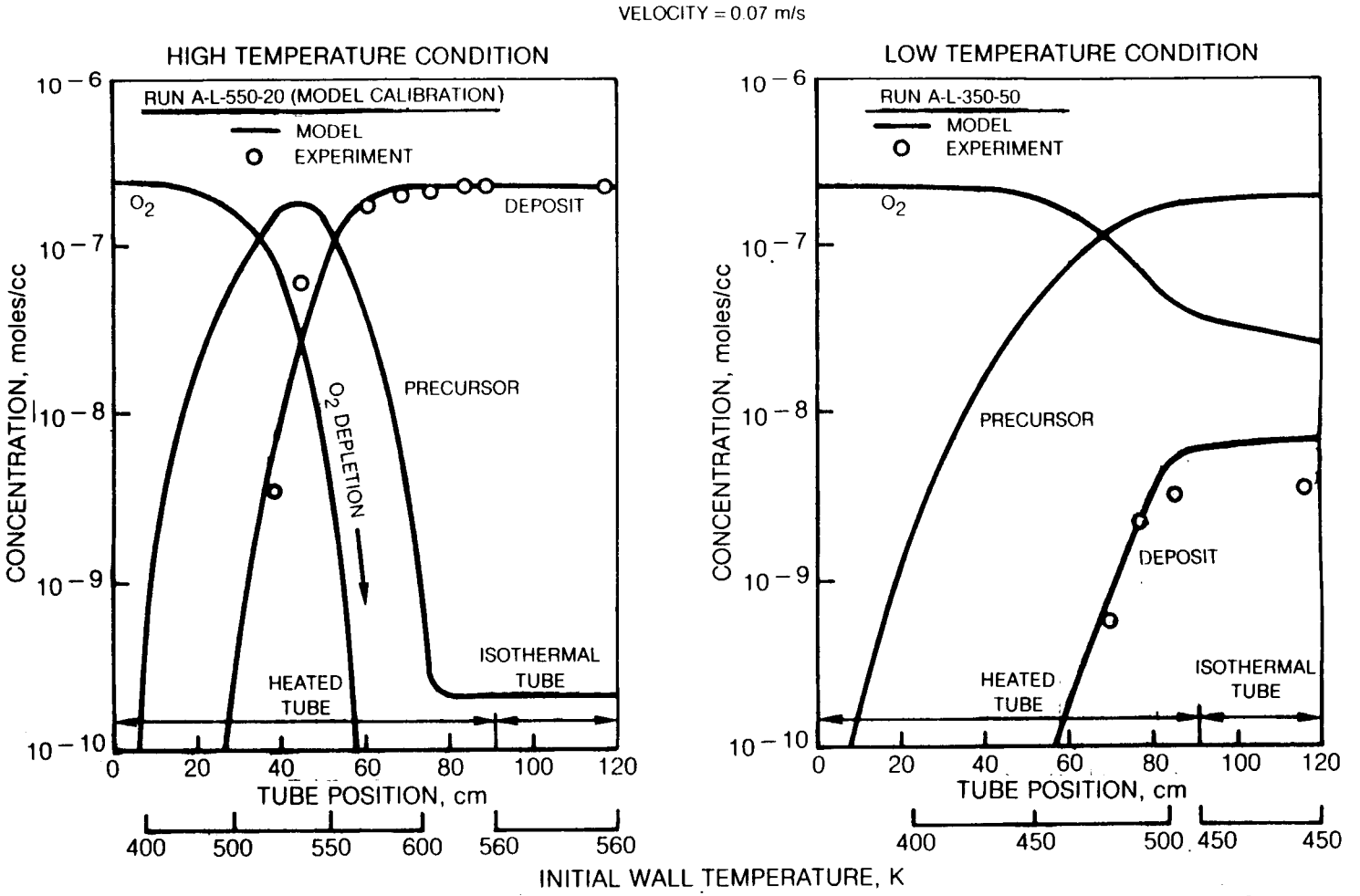

Figure 22. Predicted and Measured Deposit Species Concentration-Time Histories for Jet A Flowing in Tubes

85-3-68-14

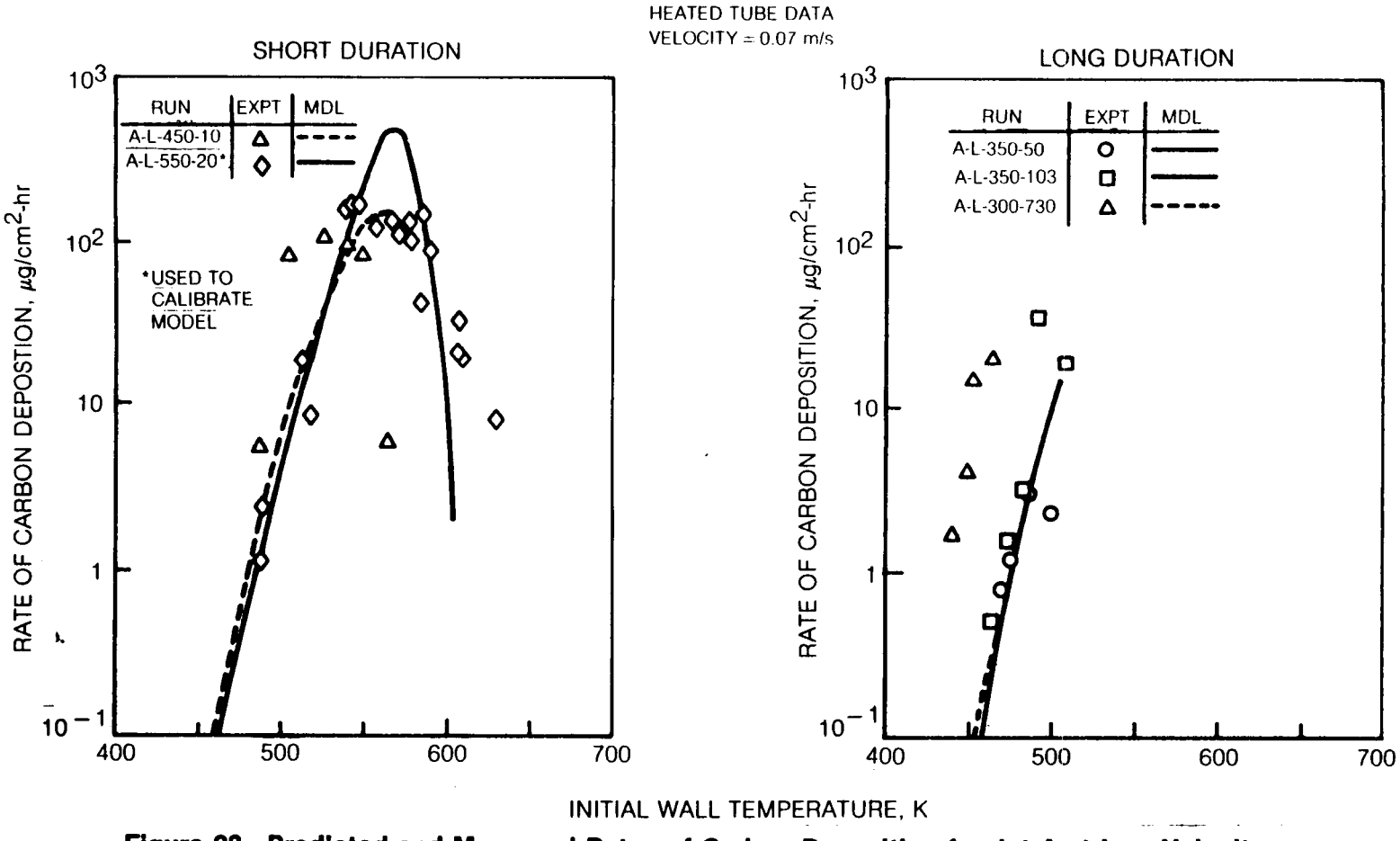

Figure 23. Predicted and Measured Rates of Carbon Deposition for Jet A at Low Velocity

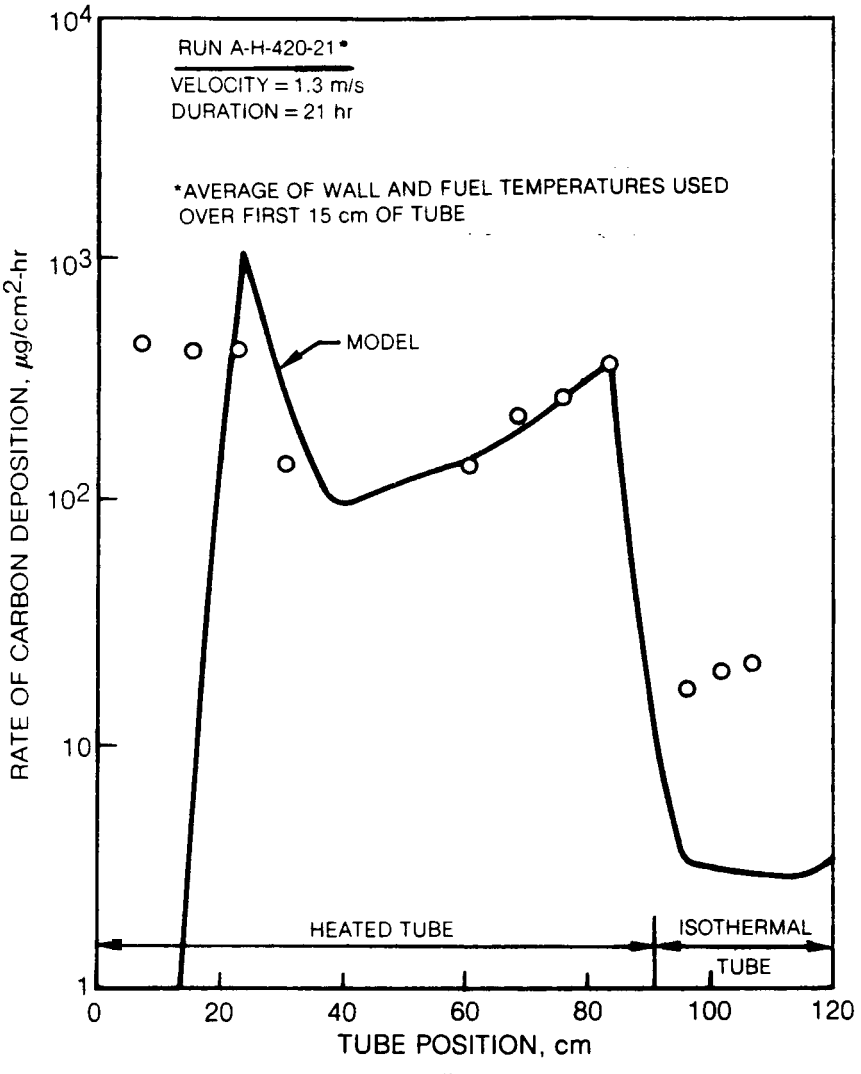

Figure 24. Predicted and Measured Carbon Deposition Rates for Jet A at High Velocity

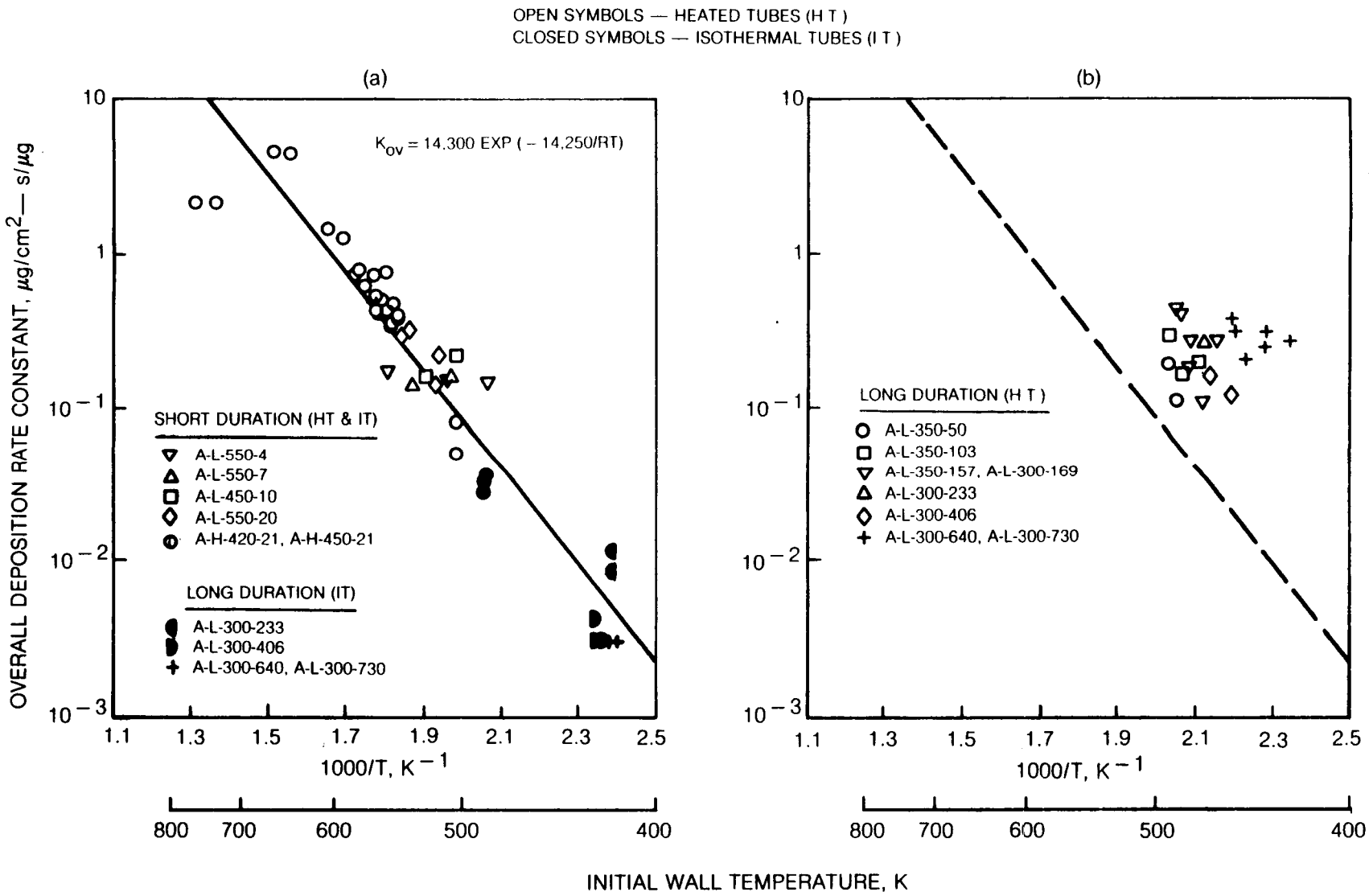

Figure 25. Overall Deposition Rate Constants for Jet A

85-3-68-1

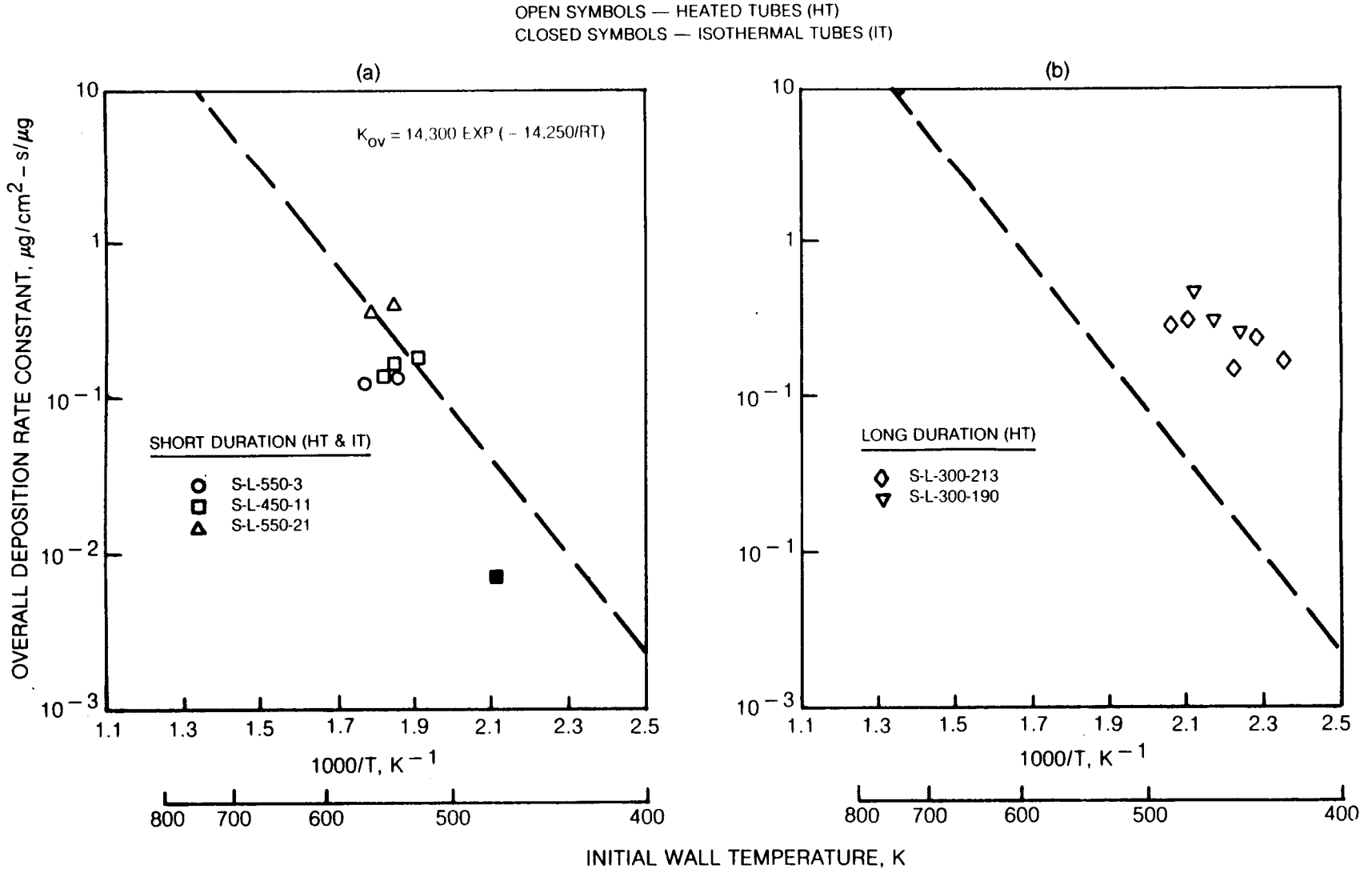

Figure 26. Overall Deposition Rate Constants for Suntech A